INVESTIGATION OF VORTEX WAKE STABILITY NEAR THE GROUND

I. H. Tombach, et al

AeroVironment, Incorporated

Prepared for:

Air Force Office of Scientific Research

31 July 1975

FINAL REPORT
AV FR 538

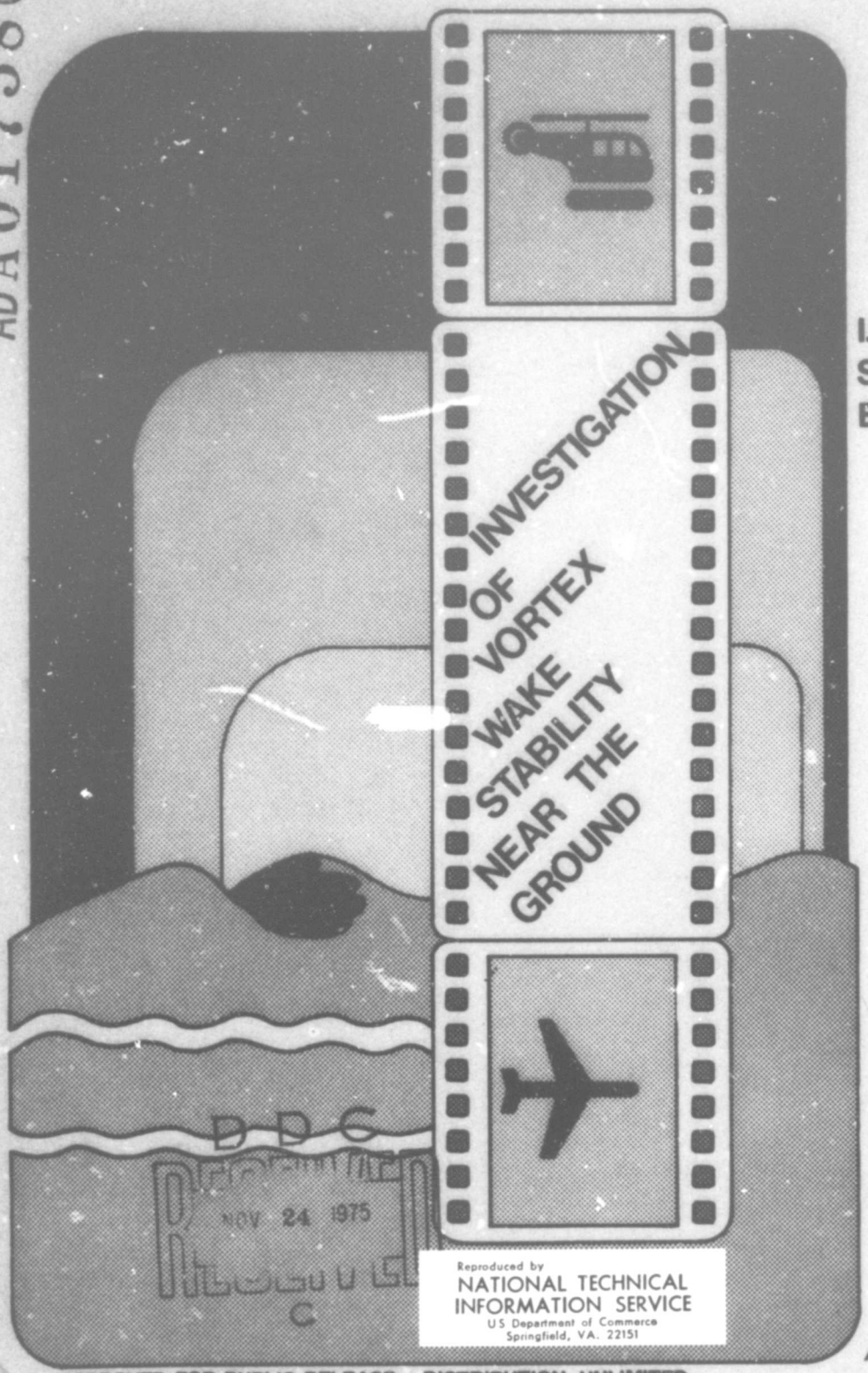

I.H. TOMBACH
S.C. CROW
E.R. BATE, JR.

PREPARED
FOR
AIR FORCE
OFFICE OF
SCIENTIFIC
RESEARCH

AEROVIRONMENT

Qualified requestors may obtain additional copies from the Defense Documentation Center; all others should apply to the National Technical Information Service.

Conditions of Reproduction

Reproduction, translation, publication, use and disposal in whole or part by or for the United States Government is permitted.

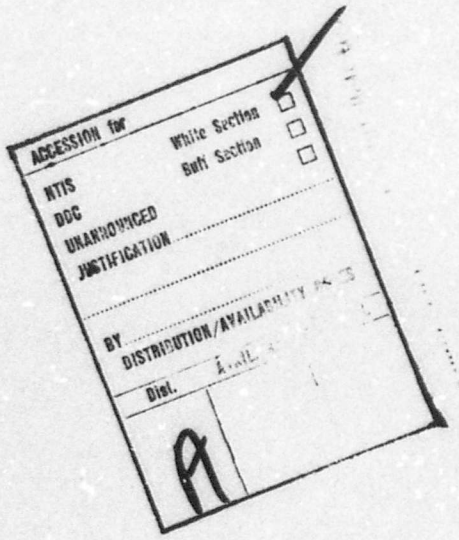

AV FR 538

Final Report

INVESTIGATION OF VORTEX WAKE STABILITY NEAR THE GROUND

by

I. H. Tombach, AeroVironment Inc.
S. C. Crow, Poseidon Research
E. R. Bate, Jr., AeroVironment Inc.

Prepared for

Air Force Office of Scientific Research
1400 Wilson Boulevard
Arlington, Virginia 22209

Under

Contract F44620-74-C-0058

by

AeroVironment Inc.
145 Vista Avenue
Pasadena, California 91107

31 July 1975

(C)

ABSTRACT

The sinuous mutual induction instability of a vortex pair has been investigated theoretically and experimentally in atmospheric conditions which prevail near the ground, thereby extending previous work of Crow and Bate for the same instability aloft. Two theoretical models were developed -- one for a vortex pair in the constant stress layer of the atmospheric boundary layer, and the second for a vortex interacting with its image when in ground effect.

The theoretical results show that the proximity of the ground shortens wake lifetime by up to 10% compared to the results aloft. The experimental data agrees satisfactorily with the theoretical predictions. The experiments also show that the rate of separation of two vortices in ground effect slows dramatically as the vortex spacing increases. A decay in vortex circulation resulting from vorticity generation at the ground is hypothesized as the cause for this.

PREFACE

The work performed on this study was one element of a continuing series of research programs underway at AeroVironment to investigate fundamental aspects of aircraft vortex wake interactions with the atmosphere under the sponsorship of AFOSR, the Department of Transportation, and the National Aeronautics and Space Administration. Although this particular study stands alone and was not performed in conjunction with other investigations (unlike the situation with recent previous work for AFOSR), it relies heavily on the expertise, equipment, and techniques which were developed during those previous projects.

The Principal Investigator for this work was Dr. Ivar Tombach. The theoretical analysis of wake instability in ground effect was performed by Dr. Steven Crow of Poseidon Research, under subcontract to AeroVironment. Mr. Edward Bate managed the field program, the analysis of its results, and their correlation with the theoretical work.

The flight test operations were performed by Flight Systems, Inc., with Mr. James Pearce flying the vortex generating aircraft and coordinating all aspects of FSI's performance. The extremely important weather forecasts required for flight operations were provided by Mr. John Aldrich.

TABLE OF CONTENTS

UNCLASSIFIED

SECURITY CLASSIFICATION OF THIS PAGE (When Data Entered)

REPORT DOCUMENTATION PAGE		READ INSTRUCTIONS BEFORE COMPLETING FORM
1. REPORT NUMBER AFOSR - TR - 75 - 1501	2. GOVT ACCESSION NO.	3. RECIPIENT'S CATALOG NUMBER
4. TITLE (and Subtitle) INVESTIGATION OF VORTEX WAKE STABILITY NEAR THE GROUND		5. TYPE OF REPORT & PERIOD COVERED FINAL 1 Feb 1974 - 31 March 1975 6. PERFORMING ORG. REPORT NUMBER
7. AUTHOR(s) I H TOMBACH S C CROW E R BATE, JR		8. CONTRACT OR GRANT NUMBER(s) F44620-74-C-0058
9. PERFORMING ORGANIZATION NAME AND ADDRESS AEROVIRONMENT INC 145 VISTA AVENUE PASADENA, CALIFORNIA 91107		10. PROGRAM ELEMENT, PROJECT, TASK AREA & WORK UNIT NUMBERS 681307 9781-02 61102F
11. CONTROLLING OFFICE NAME AND ADDRESS AIR FORCE OFFICE OF SCIENTIFIC RESEARCH/NA 1400 WILSON BOULEVARD ARLINGTON, VIRGINIA 22209		12. REPORT DATE July 1975 13. NUMBER OF PAGES 75
14. MONITORING AGENCY NAME & ADDRESS(if different from Controlling Office)		15. SECURITY CLASS. (of this report) UNCLASSIFIED 15a. DECLASSIFICATION/DOWNGRADING SCHEDULE

16. DISTRIBUTION STATEMENT (of this Report)

Approved for for public release; distribution unlimited.

17. DISTRIBUTION STATEMENT (of the abstract entered in Block 20, if different from Report)

18. SUPPLEMENTARY NOTES

19. KEY WORDS (Continue on reverse side if necessary and identify by block number)

AIRCRAFT WAKE TURBULENCE
VORTEX WAKE
VORTEX INSTABILITIES

20. ABSTRACT (Continue on reverse side if necessary and identify by block number)

The sinuous mutual induction instability of a vortex pair has been investigated theoretically and experimentally in atmospheric conditions which pervail near the ground, thereby extending provious work of Crow and Bate for the same instability aloft. Two theoretical models were developed -- one for a vortex pair in the constant stress layer of the atmospheric boundary layer, and the second for a vortex interacting with its image when in ground effect. The theoretical results show that the proximity of the ground shortens wake lifetime by up to 10% compared to the results aloft. The experimental data agrees satisfactorily with

DD FORM 1 JAN 73 1473 EDITION OF 1 NOV 65 IS OBSOLETE

UNCLASSIFIED

SECURITY CLASSIFICATION OF THIS PAGE (When Data Entered)

the theoretical predictions. The experiments also show that the rate of separation of two vortices in ground effect slows dramatically as the vortex spacing increases. A decay in vortex circulation resulting from vorticity generation at the ground is hypothesized as the cause for this.

1. INTRODUCTION

Vortex wakes exist in a complicated environment near the ground at airports. Winds, atmospheric stability, turbulence, and proximity of the ground plane each interact with the vortices in their own unique manner to determine the ultimate motion and lifetime of the wake. Under many situations, these factors combine to move the wake sufficiently far from the runway approach corridor or to sufficiently reduce its strength so that it does not constitute a hazard to following aircraft. Situations exist, however, where this might not be the case, and a wake can possibly linger at high strength near a runway for a long enough period to present operational problems.

Experiments have shown that vortex distortion, stretching, and instabilities result from an involved interaction of real-world effects with the wake. True vortex wake behavior near the ground can be expected to depart in both a deterministic as well as a random manner from the necessarily simple mathematical models which might describe various aspects of wake behavior. Nevertheless, correlation of theory and experiment is necessary in order to define the basic nature of wake phenomena and to enable extrapolation of the data to various operational situations.

The primary objective of the study described in this report was to study the effects of the ground plane on the sinuous instability mode of wake decay using both experimentally obtained flight test data and theoretical analysis of relevant phenomena. Experiments were performed by flying an Aero Commander 560A light twin-engine aircraft at 5 to 30 meters above the ground and observing, with instruments and photographically, the motion and breakup of the vortex system. For the theoretical work, the turbulence-driven wake instability theory of Crow and Bate (1975; revised from Lissaman,

et al, 1973) was modified to include the forcing function of typical atmospheric boundary layer turbulence as well as the effects of the subsurface image vortices.

In addition to meeting the basic objectives of the study, the experimental data illuminated other aspects of wake motion and decay. Specifically, this report then includes a preliminary examination of vortex breakdown due to "core bursting" and data on the spreading of the vortex pair due to the presence of the ground plane. These latter two phenomena, in conjunction with the linking instability, are of considerable operational significance.

In addition to the vortex properties, pertinent meteorological parameters were necessarily of interest, and so were routinely measured during the experimental phase of this program. These measurements allowed the characterization of the atmosphere in the test area and correlation of the meteorological factors of interest. Since measurements and correlations of the meteorological factors in operational situations must be made in order to provide inputs for the predictive model, a discussion of this aspect of the experimental program is also presented here.

The report begins with a discussion of the near-ground meteorological environment in Chapter 2. Subsequently, theoretical analysis of the impact of the ground plane on the vortices, directly, as well as indirectly via boundary layer meteorology, is discussed in Chapter 3. Experimental results and their correlation with the theory are presented in Chapter 4. An overall summary of the results of this study program appears in Chapter 5.

2. THE NEAR-GROUND ENVIRONMENT

In general, analytical models of aircraft wake behavior assume a uniform atmosphere or, in cases concerned with buoyancy effects, a linearly stratified atmosphere. Complexities present in a real atmosphere, such as inhomogeneities in wind and turbulence, are complex to handle and are usually ignored. Near the ground, however, the variability of atmospheric characteristics with height in the atmospheric boundary layer becomes significant for the analysis of some aspects of wake behavior. This is especially true for those elements influenced by turbulence or atmospheric stability, both of which are strongly affected by the presence of the ground.

Since the ground surface generally absorbs solar radiation more strongly than the air above it, it becomes hotter than the air during sunlit periods and thus, by conduction, heats the air in contact with it. This heating results in an unstable lapse rate and, consequently, in the generation of thermal plumes and turbulence. During the night, on the other hand, surface cooling stabilizes the lapse rate and suppresses turbulence.* These effects can be very strong in the bottom few tens of meters of the atmosphere, particularly in the absence of wind.

Turbulence aloft is generally isotropic to a fair degree of approximation (MacCready, 1962) for wavelengths less than a few hundred meters. As the ground is approached, its presence suppresses the longer wavelengths of vertical turbulence motion (those of a scale larger than the order of half the height above the surface) but has little effect on the horizontal motions. Obviously, very near the ground, then, the motion of the air is predominantly horizontal, with very little vertical activity.

*See, however, the discussion in Tombach, et. al., 1974, where stability-induced drainage flows generated turbulence.

At appropriate heights above the surface the stability effects and turbulence suppression caused by ground proximity can act either in concert or at cross purposes. To illustrate actual behavior, Figure 2-1 shows data on turbulence at 4 m above the ground which was taken at El Mirage Dry Lake during one day of the field experiments described in Chapter 4. Plotted are the ratio of r.m.s. turbulence velocities in the horizontal direction, σ_v, traverse to the flight path, to those in the vertical direction, σ_w. The turbulence was measured with low response threshold propeller anemometers, and the signal was processed by a sigma meter (Jones and Pasquill, 1962) which passed (with less than 3 dB of attenuation) wavelengths shorter than 345 seconds in period* and computed the r.m.s. values with a smoothing time constant of 750 seconds. The horizontal component anemometer was oriented in a north-south direction, perpendicular to the flight path, thus the crosswind component given later in Table 4-3 is just the velocity v, while the wind velocity component along the flight path is denoted by u. Each data point shown in Figure 2-1 is an average of the σ_v/σ_w ratio for the preceding 15 minutes.

In the early morning hours when significant stability prevailed (with an inversion of strength 4.6°C per 100 m at 8 m above the surface) the ratio σ_v/σ_w was very nearly unity (ranging from 0.8 to 1.25) in the presence of negligible wind, most of which was along the flight path and thus perpendicular to the direction sensed by the anemometer. The ratio remained near unity until about 0830, increasing slightly as the wind direction changed to northerly. A change in wind direction to a crosswind occurred by the time runs 4 through 6 took place around 0830 and the wind speed began to increase shortly thereafter, resulting

*Corresponding in these tests to lengths less than 35 to 200 m, depending on wind speed.

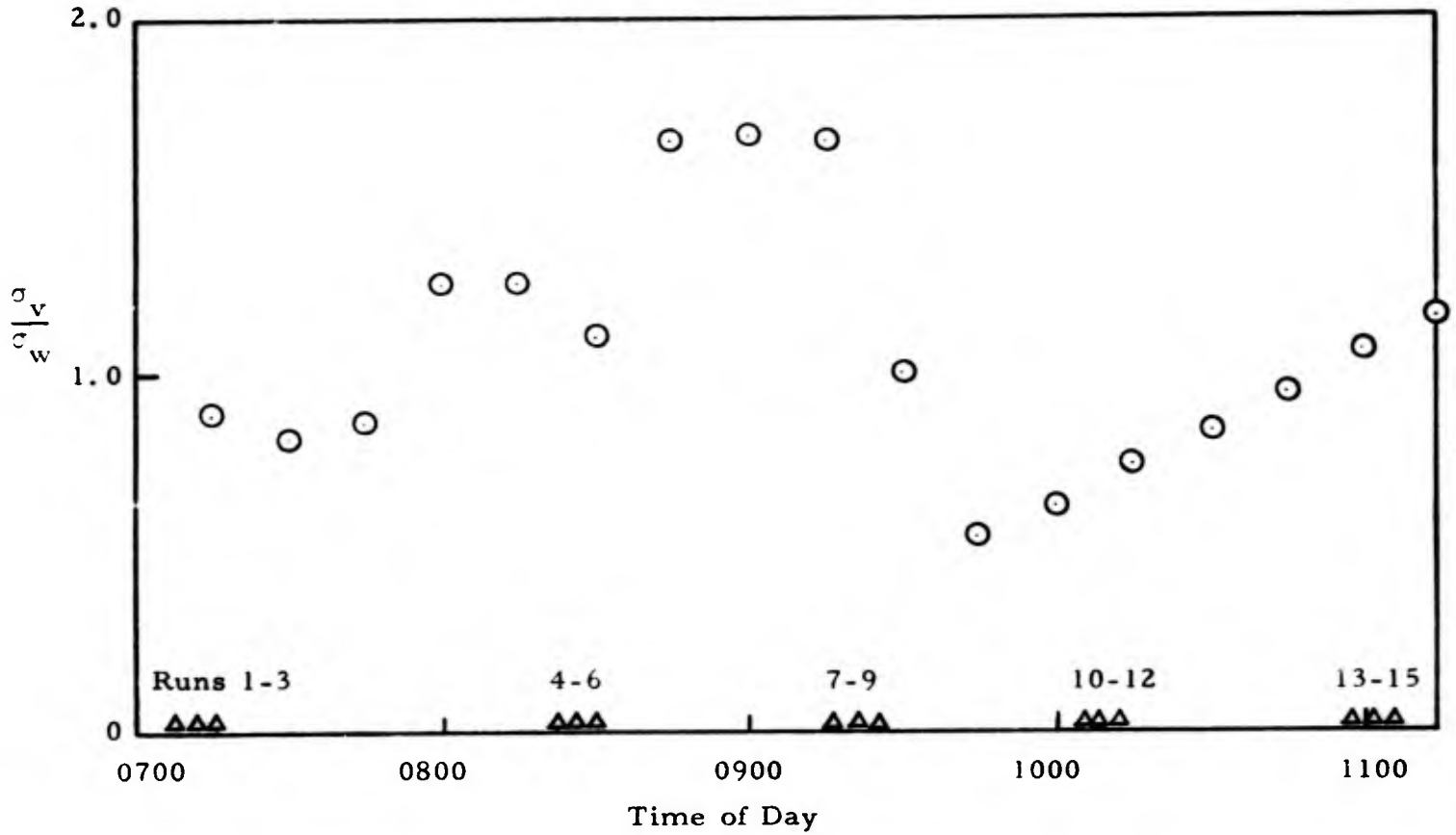

FIGURE 2-1. Inhomogeneity of how-level turbulence on 11 February 1975 at 4 m above El Mirage Dry Lake. The times at which the test runs were made with the vortex generator aircraft are indicated.

in a σ_v/σ_w ratio of 1.7 from 0830 to 0900. The wind speed decreased to almost total calm after 0900 and thermal activity began to increase σ_w then, so that σ_v/σ_w reached a low of 0.5 at 0945, at which time the lapse rate at twice the anemometer height was neutral. Increasing winds after that time caused the monotonically increasing trend shown in Figure 2-1, with σ_v/σ_w again slightly more than unity after 1100 as mechanical turbulence again dominated.

This discussion shows quantitatively that turbulence near the ground is inhomogeneous, particularly in the calm, stable morning hours, and that the lateral turbulence intensity differed from the vertical by a factor of up to 2 at the location shown here, for the scales considered. Generally the inhomogeneity would be less at higher elevations, although the eddy length scale of interest must be less than about twice the height above the ground for relatively homogeneous conditions to prevail at most times. A quantitative description of the variability of turbulence with height is desirable for the development of theoretical models of wake behavior near the ground. Such models, which exist for many atmospheric conditions, are described below.

2.1 Conditions in the Surface Layer

The earth's boundary layer, whose height ranges from 0.1 to 10 km, with 1 km a common daytime height, is commonly divided into two parts: (1) the surface boundary layer, across which the vertical fluxes are constant, and (2) the total boundary layer, whose top is found where the fluxes become small. The height of the surface layer is typically between 20 and 200 meters, with the smallest values occurring in the most stable conditions.

Within this constant flux (and thus constant stress) layer near the ground, a quantitative theory developed by Monin and Obukhov

(1954) can be applied to the turbulence there. Their similarity theory shows that

$$\frac{\kappa z}{u^*}\chi = S\left(\frac{z}{L}\right)$$

where χ is the turbulence characteristic of interest, S is a universal function, z is the height above the ground, L is the Monin-Obukhov length, κ is the von Karman constant ($\kappa = 0.4$), and u^* is the friction velocity ($u^{*2} = \overline{u'w'}$). L is a parameter related to the lapse rate of the atmosphere, with $z/L \approx 0$ corresponding to neutral conditions, $z/L > 0$ to stable stratification, and $z/L < 0$ (i.e., $L < 0$) to unstable conditions.

The forms of the universal function S for $\chi = \sigma_w$ and ϵ are of interest here; they must be determined experimentally or by appropriate theoretical inference. In the case of σ_w, it has been found experimentally that σ_w is relatively invariant with height and stability in the surface layer where, indeed, the vertical fluxes are constant. One recent experimental study (McBean, 1971) finds $\sigma_w/u^* \approx 1.55 \pm .15$ for z/L ranging from -0.75 to +10. Other experimenters have found mean values of σ_w/u^* between 1.2 and 1.4 in neutral atmospheres, with higher values as the stability is increased.

The discussion so far has been confined to conditions where turbulent mixing arises as a consequence of the normal generation processes in the shearing flow in the boundary layer, which require that there be an adequate flow over sufficiently rough terrain. For more unstable conditions, free convection begins to dominate and the scaling changes. In free convection conditions (say, $z/L \lesssim -.5$) Lumley and Panofsky (1964) have predicted theoretically that $\sigma_w/u^* \sim |z/L|^{1/3}$, i.e., it increases very gradually with height.

Another quantity of interest is the turbulence dissipation rate, ϵ , for turbulence in the inertial subrange. Aloft, well away from the ground, it has been found (MacCready, 1962) that the classic inertial subrange description by Kolmogorov is a surprisingly good representation of the atmosphere. Kolomogorov's similarity hypothesis results in the conclusion that all statistical properties of turbulence relate only to ϵ when the turbulence is within the range of scales called the inertial subrange, which ranges typically from wavelengths of a few centimeters to many hundreds of meters, and within which isotropy prevails. Studies have shown (MacCready, 1962, and the discussion by Lumley and Panofsky, 1964, pp. 166-167) that near the ground the inertial subrange spectrum laws seem reasonably valid even at wavelengths about twice the height of observation (and still longer in unstable cases). It may seem surprising that wavelengths greater than z can actually show statistical energy isotropy and agree with the simplified spectrum laws, but it should be remembered that the turbulence formulas deal with energies and velocities, not displacements, and so isotropy of energy for the three directional components for, say, 100 m horizontal wavelengths may be reasonable at a height of only 50 m.

Below the height at which the simple Kolmogorov spectrum holds, the suppression of the vertical motion by the ground changes the relationships between the dissipation rate and the energy contained in each of the various components of turbulence. The relationship between ϵ and z has not been defined as unambiguously as that for σ_w has. The reasons for this can be viewed from two perspectives. On the one hand, in the inertial subrange ϵ is related to the total kinetic energy contained in σ_u^2 , σ_v^2 , and σ_w^2 . There is no theory, however, which relates the lateral turbulence to z/L , there are questions as to whether such a relation should exist, and experimental data shows large scatter and a strong dependence on local roughness features. Indications are thus that a similarity law cannot be formally constructed for ϵ .

From a different perspective, in a steady-state situation the dissipation ϵ equals the mechanical production of energy plus the buoyant production less the flux divergence of turbulent energy upward. The extent of the buoyancy and divergence terms is difficult to define, and one not totally irrational assumption is that they approximately cancel. This approach, which is used in the next section, gives $\epsilon^{1/3} \sim z^{-1/3}$. Experiments have shown this to be an acceptable formulation for a wide range of atmospheric stabilities (Pasquill, 1972) and more refined formulations are available if needed.

The final universal function of interest is that of $\partial U/\partial z$. Various derivations (Lumley and Panofsky, 1964; Fieldler and Panofsky, 1972) show that, for forced convection, the wind profile is given by

$$U = \frac{u^*}{\kappa} \left(\ell n \frac{z}{z_o} - \Psi \left(\frac{z}{L} \right) \right) + C_z \qquad (2.1)$$

where the linear increase C_z due to the Coriolis force is negligible below $z = 30$ m or so and $\Psi(z/L)$ is zero for neutral conditions, negative for stable conditions, and positive for unstable conditions. Values for Ψ and C are given in the references just cited, respectively. In highly unstable conditions with free convection and moderate wind speeds mixing length theory gives $U \sim z^{1/3}$.

In neutral conditions near the ground Equation (2.1) gives

$$U = \frac{u^*}{\kappa} \ell n \frac{z}{z_o} \quad , \qquad (2.2)$$

the well known logarithmic profile for the lower portion of a turbulent boundary layer.

This brief general discussion can be used as a basis for the specific formulations which follow in subsequent sections for application to the description of vortex behavior near the ground. For a more in-depth discussion of the general situation in the bottom several tens of meters of the planetary boundary layer, the report by Lissaman, et. al. (1973) contains a comprehensive review with a vortex wake perspective.

One important point concerning the use of these formulas cannot be overemphasized, however. The formulas require a constant stress layer, which in turn requires a wind flow over terrain of sufficient roughness to generate turbulence and stability low enough to permit upward diffusion of this turbulence. Thus, when the surface roughness is small and/or the atmospheric stability is great, the thickness of this constant stress layer can be small indeed. Many situations of operational interest occur in just these conditions, possibly with low wind speeds also, in which case there may be a significant section of the lower atmosphere above the very thin constant stress layer where the presence of the ground still affects turbulence spectra but within which no simple formulation of turbulence spectra can be derived.

2.2 Turbulence Characteristics Affecting the Wake Lifespan of a Descending Wake

Crow and Bate (1975) have argued that eddies in the Kolomogorov inertial subrange are responsible for exciting a mutual induction instability which results in the now well-known decay of a parallel vortex pair into a chain of vortex rings. Their theory is valid when the vortices are at altitudes greater than the instability wavelength, so that the inertial subrange concepts of Kolmogorov hold. The wavelength λ of the maximally amplified mode of instability was

shown to satisfy the formula $\lambda = 8.6\, b_v$, where b_v is the vortex spacing. For a Boeing 747, b_v is about 34 m and λ is thus 288 m, while for the aircraft used in this study $b_v = 10$ m and $\lambda = 86$ m. Assuming that the simple scaling laws for isotropic turbulence hold down to a height $h = \lambda/2$, then the derivation of Crow and Bate can be used down to about 144 and 43 m, respectively, for these two aircraft. Below this height, down to the level where the influence of the image vortices begins to be felt at, say, $h \approx b_v$, there is a region where the kinematics of the Crow and Bate formulation are still correct, but the effect of altitude on the turbulent forcing function needs to be considered. Here that turbulent forcing function will be defined; its impact on wake lifespan will be discussed in Chapter 3.

The coordinates for describing the turbulent field are illustrated in Figure 2-2. The coordinate x is opposite to the direction of flight, y is the spanwise coordinate, and z is the vertical coordinate with an origin at the ground. The interest here is in relevant turbulence properties at the altitude $z = h$ of the vortex wake.

Crow and Bate show that the mutual induction instability at high altitudes is dominated by the vertical component of turbulent velocity along the centerline of the wake, $w(x, 0, h)$. A statistical quantity of major importance is the correlation function

$$R_w(r, h) = \langle w(x, 0, h)\, w(x+r, 0, h) \rangle \qquad (2.3)$$

where r is a separation in the x-direction, and the angle brackets denote an ensemble average. $R_w(r, h)$ measures the intensity of the vertical velocity fluctuations and also their correlation along the vortex wake. Closely related is the turbulence spectrum $W(k, h)$, the Fourier transform of $R_w(r, h)$:

$$R_w(r, h) = 2 \int_0^\infty W(k, h) \cos(kr)\, dk \quad . \qquad (2.4)$$

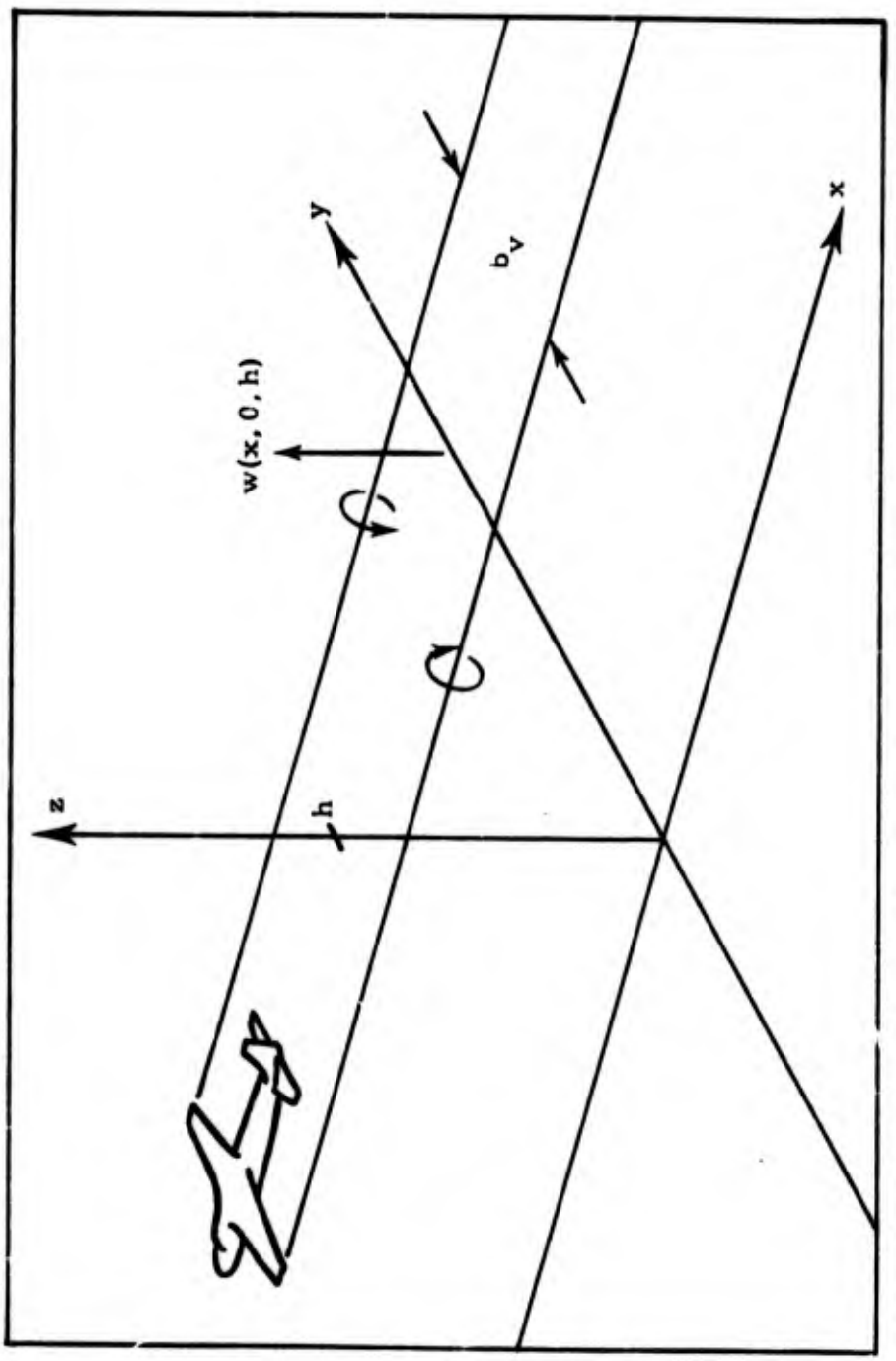

FIGURE 2-2. Coordinates for the analysis of a descending vortex wake.

For large values of kh , the product of wavenumber and altitude, W(k, h) has the form appropriate for the Kolmogorov inertial subrange:

$$W(k,h) = \frac{12}{55}\,\alpha\,[\epsilon(h)]^{2/3}\,k^{-5/3} \quad . \qquad (2.5)$$

The constant α is empirically determined to be around 1.5 for k expressed in radians per unit length and W defined by the result*

$$\int_0^\infty W(k,h)\,dk = \frac{1}{2}\langle w^2\rangle \quad . \qquad (2.6)$$

The quantity $\epsilon(h)$ is the rate of turbulent energy dissipation per unit volume, which was discussed previously in Section 2.1. Crow and Bate used Equation (2.5) as their turbulent input spectrum.

For the region below where Equation (2.5) applies, where now kh is of order unity or less, the concepts of the constant stress or "log" layer of the boundary layer can often be invoked since the heights of interest (less than 144 and 43 m respectively for the Boeing 747 and the Aero Commander 560A) are frequently, though not always, within the 20 to 200 m depth of this layer. In this layer, whenever wind-driven turbulence production dominates any thermal effects, the largest turbulence length scales are proportional to the distance z from the ground, and velocity scales are proportional to the friction velocity u* , defined as the square-root of wind stress τ_o at the ground divided

---

*There are many chances for confusion here. Meteorologists often measure k in terms of cycles per unit length, in which case $\alpha = 0.45$. Also, expressions of Equation (2.6) frequently delete the factor 1/2 on the right-hand side, in which case α is twice the values given here. See Panofsky and Pasquill (1963) and Tennekes and Lumley (1972), p. 273, for discussion of these points.

by fluid density ρ :

$$u^* = (\tau_o/\rho)^{1/2} \quad . \tag{2.7}$$

From Eq. (2.2), the gradient of the mean wind velocity U(z) has the form

$$\frac{dU}{dz} = \frac{u^*}{\kappa z} \quad . \tag{2.8}$$

Assuming that energy production and dissipation balance locally in the constant-stress region, and production is the product of Reynolds stress and mean velocity gradient, then

$$\epsilon = u^{*2} \frac{\partial U}{\partial z} \quad , \tag{2.9}$$

and from Eq. (2.7) and (2.8),

$$\epsilon(h) = \frac{u^{*3}}{\kappa h} \tag{2.10}$$

at height $z = h$.

The spectrum W must scale on the same parameters h and u^* , and dimensional reasoning implies that

$$W(k, h) = u^{*2} h \, \mathcal{W}(kh) \tag{2.11}$$

for some universal function $\mathcal{W}(kh)$. Comparing Equations (2.5) and (2.11), for example, we find that

$$\mathcal{W}(kh) \to 0.593 \, (kh)^{-5/3}$$

as $(kh) \to \infty$,

in the Kolmogorov inertial subrange. To determine $\mathcal{N}$ for (kh) of order unity or less requires recourse to experiment.

Fortunately a great deal of experimental data is available for the spectrum of vertical turbulent fluctuations, because vertical currents are responsible for gust loads on airplanes as well as for air pollutant dispersion. The Busch and Panofsky (1968) spectral shape

$$\mathcal{N}(kh) = \frac{B}{A+(kh)^{5/3}} \tag{2.12}$$

satisfactorily fits the data. From the Kolmogorov limit, Eq. (2.11), we already know that B is 0.593. The dimensionless parameter A can then be obtained by performing the integration

$$\sigma_w^2 = \langle w^2 \rangle = 2\int_0^\infty W(k,h)\, dk = \frac{2.35}{A^{2/5}}\, u^{*2} \quad , \tag{2.13}$$

and using experimental data for the ratio σ_w/u^* .

Some experimentally derived values of the ratio σ_w/u^* were discussed previously in Section 2.1. Considering all factors, including the fact that our interest is in the calmer, stabler conditions conducive to long wake life, suggests that choosing $\sigma_w/u^* = 1.55$ is reasonable. This then gives A = 1.03 and

$$\mathcal{N}(kh) = \frac{0.593}{1.03 + (kh)^{5/3}} \tag{2.14}$$

This is the equation which will be used later as the basic turbulent input spectrum over the altitude range where the ground affects the turbulence spectrum. This formula is valid near the ground, thus it is almost always correct in the very lowest part of the atmospheric

boundary layer as long as a constant stress layer exists. It also matches the Kolmogorov spectrum as $kh \to \infty$. Thus, even if the constant stress layer similarity formulas do not apply all the way from the ground up to where the effects of the ground can be ignored, this formula fairs smoothly through any intermediate levels and is thus a reasonable representation for all heights.

2.3 Lateral Turbulence Characteristics Very Near to the Ground

The turbulence property relevant to vortex lifespan analysis changes as the vortices enter ground effect. There the vortices interact strongly with their images and separate laterally as they settle down to an altitude

$$h = b_v/2 \quad , \tag{2.15}$$

as explained in detail elsewhere in this report. After the brief interaction among the vortex and image pairs at the onset of ground effect, a vortex and its image move outward as though they were an isolated pair, except that motion takes place in the y instead of the z-direction.

For an isolated vortex moving along the y-axis under the induction of its image, the y-component of turbulent velocity is responsible for exciting the instability. Thus the forcing velocity of interest is now $v(x, y, b_v/2)$, where y is constant along the vortex, and the altitude is constrained to be $b_v/2$. Again the important turbulence characteristics are a correlation function

$$R_v(r, b_v/2) = \langle v(x, y, b_v/2)\, v\,(x+r, y, b_v/2)\rangle \quad , \tag{2.16}$$

with a spectral representation

$$R_v(r, b_v/2) = 2\int_0^\infty V(k, b_v/2) \cos(kr)\, dk \quad . \qquad (2.17)$$

The spectrum can again be written in terms of the similarity variables u^* and $h = b_v/2$ appropriate for the constant-stress region. Thus, define a universal function $\mathscr{V}$ by

$$V(k, b_v/2) = u^{*2} b_v \mathscr{V}(\beta) \quad , \qquad (2.18)$$

where β is the dimensionless wavenumber first introduced by Crow (1970):

$$\beta = kb \quad . \qquad (2.19)$$

Notice that, for simplicity, the separation b_v between the vortex and its image is being used in Eq. (2.18), rather than the vortex altitude $b_v/2$.

$V(k, b_v/2)$ must have the Kolmogorov form, Eq. (1.5), for large values of β , so

$$\mathscr{V}(\beta) \to 0.939\, \beta^{-5/3}$$
$$\text{as} \qquad \beta \to \infty \quad . \qquad (2.20)$$

That does not help us much, however, because β is 0.73 for the maximally amplified mode of instability:

$$\beta = kb = \frac{2\pi b}{\lambda} = \frac{2\pi}{8.6} = 0.73 \quad .$$

Unlike the situation for vertical gusts, moreover, few experimental data are available for the correlation functions and spectra of horizontal velocity fluctuations. A final difficulty is that $\mathcal{V}(\beta)$ is likely to depend on the alignment of the wind with respect to our vortex-oriented coordinates. To obtain definite results, we shall assume here that the wind is blowing in the y-direction, exactly transverse to the vortex wake. That is the worst possible case from an operational point of view, since a traverse wind can stop one of the vortices over the runway.

To deduce the spectrum $V(k, b_v/2)$, the plot of $R_v(r,h)$ in Figure 2-3, derived from Tritton (1967), can be used as a starting point. Now, the spectrum is defined by

$$\sigma_v^2 = \langle v^2 \rangle = 2\int_0^\infty V(k, b_v/2)\, dk$$

$$= 2\, u^{*2} \int_0^\infty \mathcal{V}(\beta)\, d\beta \quad . \qquad (2.21)$$

Experiments show that a simple expression of the form $\sigma_v = C\, u^*$ (where, now, v is the along-wind component) is not universally possible, for lateral turbulence need not scale according to the similarity laws of vertical turbulence. Consequently there is considerable variability in the values determined for C, with numbers ranging from 1.6 on up to above 3 depending on the measurement site and prevailing stability (Busch, et al, 1973). A rational choice is one somewhere in the midpoint of the major data concentration from C = 1.8 to 2.3, so $C \approx 2.1$ will be used here. This gives.

$$\sigma_v^2 \approx 4.5\, u^{*2}$$

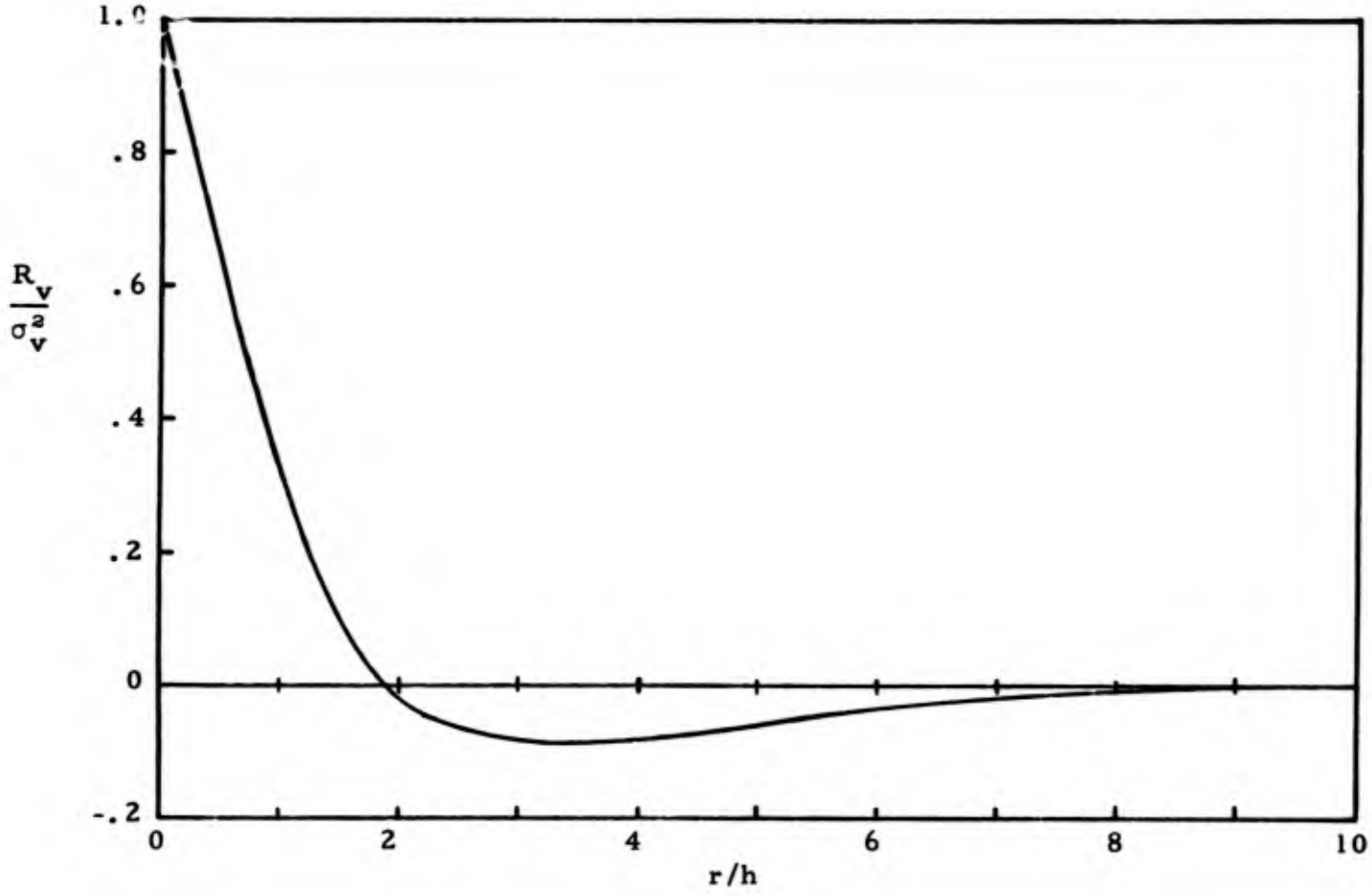

FIGURE 2-3. "Best" traverse correlation function for the windward component of the turbulent velocities, Tritton (1967).

as an integral condition, from which application of Eq. (2.21) gives

$$\int_0^\infty \gamma(\beta)\, d\beta = 2.25 \quad . \tag{2.22}$$

To progress further, more information about the shape of the spectrum $V(k, b_v/2)$ is needed. In principle the spectrum could be obtained from Figure 2-3 by numerical evaluations of the Fourier inversion integral

$$V(k, b_v/2) = \frac{1}{\pi} \int_0^\infty R_v(r, b_v/2) \cos(kr)\, dr \quad . \tag{2.23}$$

An approximation adequate for this analysis can be inferred from the spectral shape $\gamma(\beta)$ by noting two facts in addition to the constraints in Eq. (2.20) and (2.23). First, the value of the spectrum at $k = 0$ can be obtained by planimeter integration of Figure 2-3 itself, giving

$$V(0, b_v/2) = \frac{1}{\pi} \int_0^\infty R_v(r, b_v/2)\, dr$$

$$= 0.17\, \sigma_v^2 (b_v/2) \quad ,$$

from which

$$\gamma(0) = 0.38 \tag{2.24}$$

according to Eqs. (2.18) and (2.22). Second, the correlation function $R_v(r, h)$ has a pronounced negative minimum at $r = 3.5\, h$, suggesting a spectral peak at a wavelength around twice that value, i.e., at $7\, h = 3.5\, b_v$, which in turn implies that $\gamma(\beta)$ should have a maximum at

$$\beta = kb_v = \frac{2\pi}{(3.5\, b_v)} b_v = 1.8 \quad . \qquad (2.25)$$

The spectral plot in Figure 2-4 has been drawn to conform with Eqs. (2.20), (2.22), (2.24), and (2.25). The plot is an approximate Fourier transform of the correlation function in Figure 2-3, but the approximation is probably at least as good as the data from which Figure 2-3 was derived. Indicated on the figure are two asymptotic curves which will be used in subsequent analysis of wake instability near the ground.

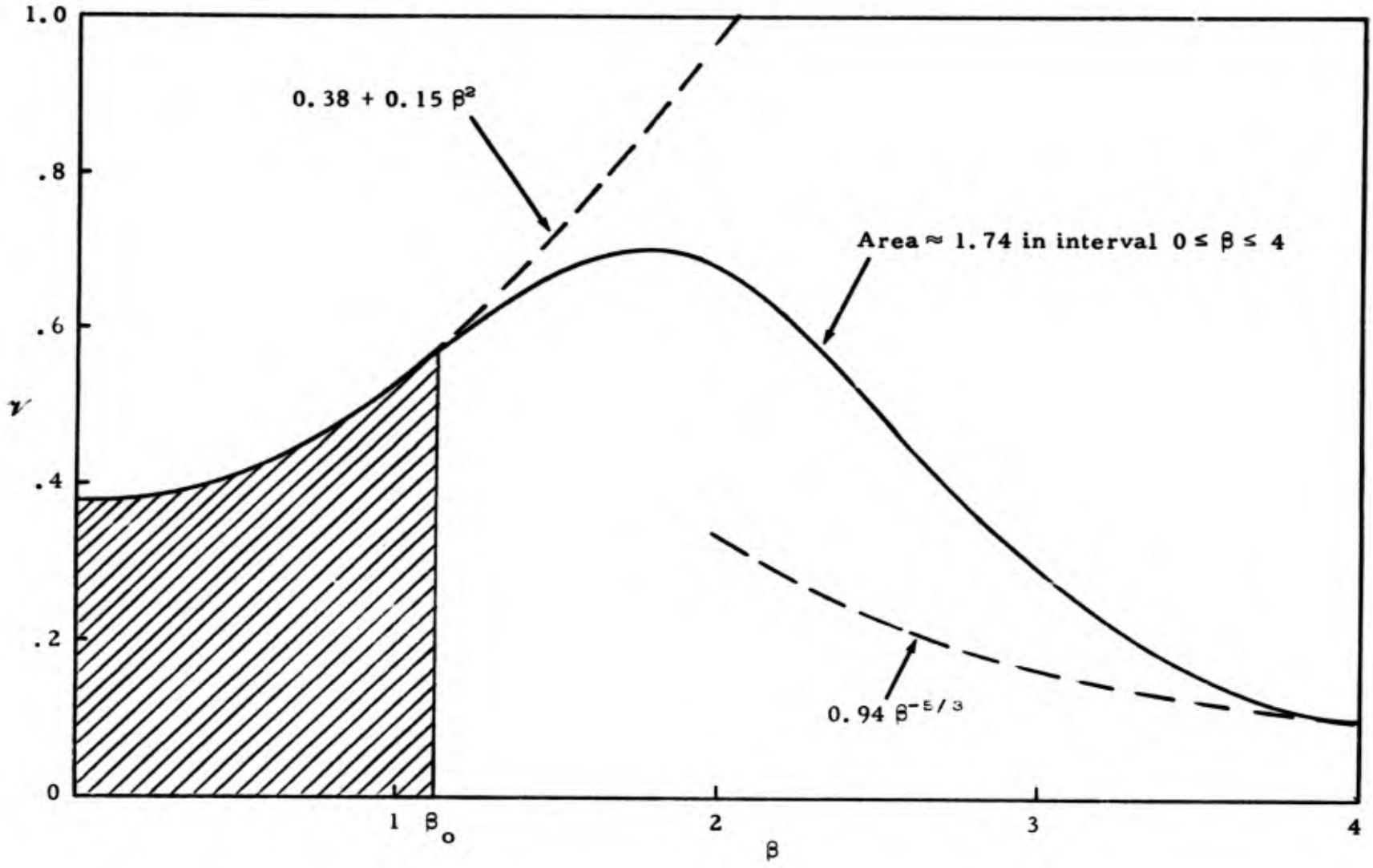

FIGURE 2-4. Spectrum estimate for horizontal turbulence at height $b_v/2$. The asymptotic curves and the shaded region are used in the stability analysis in Section 3.3.

3. MODELING OF WAKE BEHAVIOR NEAR THE GROUND

The vortex wake from a large transport aircraft is almost never generated in a totally predictable, "wind tunnel-like" environment. All of the statistical vagaries of the atmosphere are present, superimposed in a highly non-linear manner on the mutual and self-induced motions of the vortex pair. On the other hand, common theoretical formulations of vortex motion are limited to the extent that they usually only treat a single aspect of vortex behavior. Thus, the comparison of experimental data obtained in a real atmosphere with a given theory or analytical representation must involve the use of some form of interpretation, to account for the many other variables not treated in the analysis.

The vortex wake generated near an airport involves many more complicating factors than just random effects of the atmosphere, however. The wake of operational concern is normally generated by an aircraft on landing approach and hence the influence of the ground on the wake is a continuously changing function of distance out from touchdown point. This is not a trivial consequence of the landing geometry, since resultant wake behavior (both motion and decay) is sensitive to the height above the ground at which the vortices were generated. Thus, the prediction of the location of a vortex (or whether it will still be there at all due to decay) depends upon the influence of the ground.

This chapter and the next present analytical and experimental information on the behavior of certain aspects of wakes in ground effect. The random action of the atmosphere is clearly evident. Deterministic elements of the atmosphere/ground/vortex interaction are identifiable, however, and form the justification for the efforts at analytical modeling of wake behavior in this chapter. The experimental data used for verifying the theory follows in Chapter 4.

3.1 Vortex Trajectories Near Ground

As is well known, vortices generated or moving into ground effect are subjected to the influence of an image vortex pair and hence move apart as they approach the ground. Figure 3-1 shows predicted trajectories for a single vortex generated at various altitudes by the Aero Commander 560A aircraft used in the experimental portion of this study. The aircraft and vortex parameters used for the calculations are given later in Table 4-1. The figure is labeled with dimensionless axes, and the trajectory data can be used for any aircraft. The speed of vortex transport depends on the circulation, however, and thus the times shown apply only for the chosen aircraft.

The figure was prepared using a computer routine to model the vortex pair and its image system in a potential flow situation. The velocity field at the vortex of interest due to the other three vortices was computed and the resultant change in geometry due to the induction velocities, and hence the motion of the vortices, was determined by time-step integration of the equations of motion (from Lamb, 1945, page 224).

From the analytical standpoint, vortices which are generated high out of ground effect ($> 2b_{ve}$,* say) descend to an altitude given by one-half their equilibrium spacing aloft. Vortices generated closer to the ground descend to distances less than one-half the equilibrium spacing, and descend little or not at all if generated below $b_{ve}/2$ above the ground. Additionally, vortices generated closer to the ground move apart at increasingly higher separation velocities. The speed of the motion scales linearly with the vortex circulation, given identical geometric conditions.

---

*b_{ve} is the vortex spacing computed from the span assuming elliptical spanwise distribution of lift, i.e., $b_{ve} = (\pi/4)\, b$.

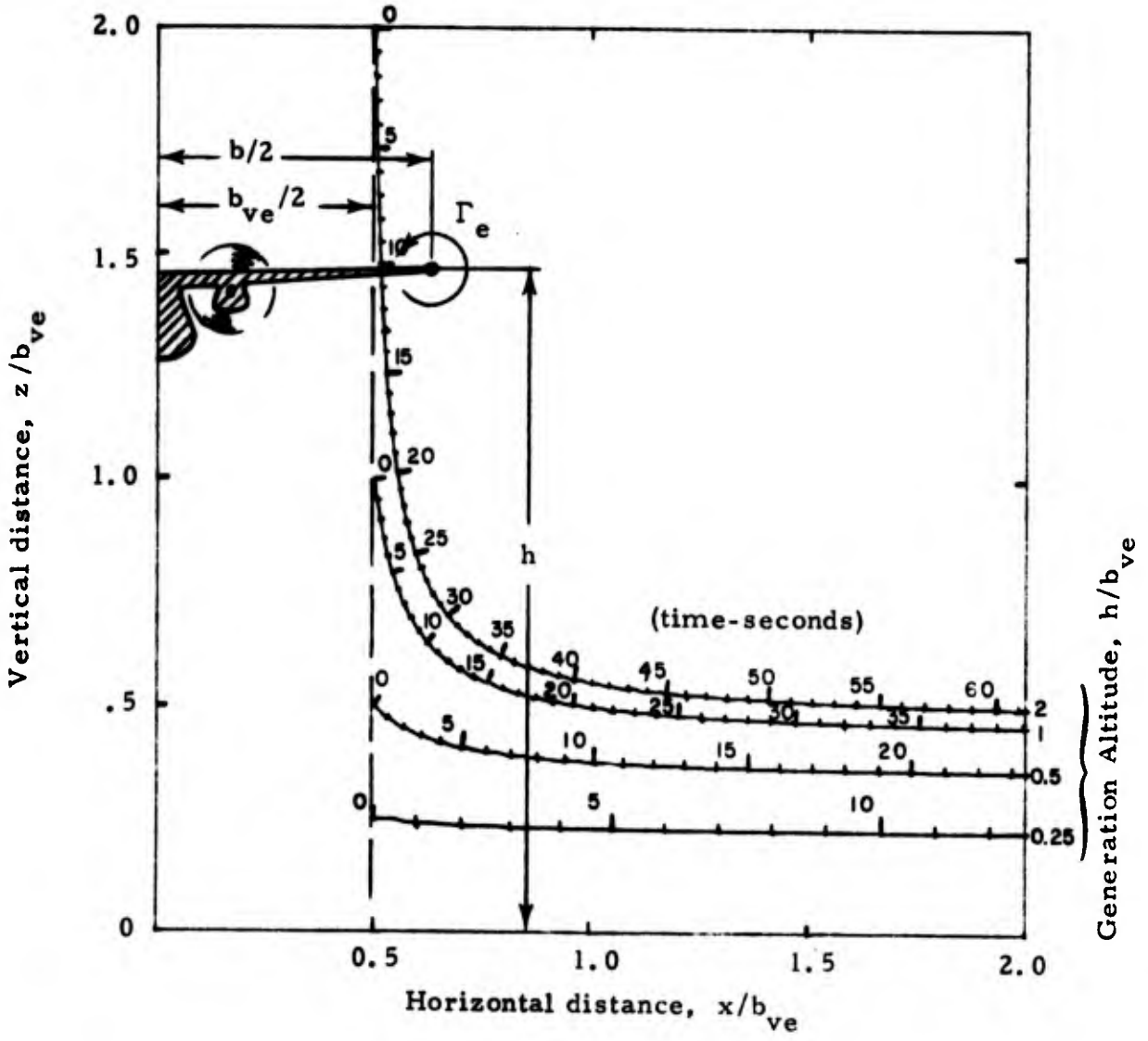

FIGURE 3-1. Vortex descent trajectories in ground effect as a function of generation altitude. Only the motion of one vortex is shown. Tick marks along the trajectories indicate time in seconds, with 5-second intervals labeled for $\Gamma_e = 40.6\ m^2\ s^{-1}$.

In an actual case, as the aircraft wing approaches the ground an increasing proportion of the lift is borne by the pressure field resulting from the downwash momentum impacting the ground, and thus the circulation required to support the aircraft will decrease. This decrease in vortex strength very near the ground for a given aircraft configuration was not considered in this calculation. The trajectories would not be altered; the velocities would be, however.

In the actual atmosphere, as the vortex descends through the various strata of the boundary layer it encounters varying turbulence levels and spectra, varying wind drift, and a continuously changing vortex spacing due to ground effect. Consequently, the fate of a prescribed segment of vortex, generated at an arbitrary height, will be difficult to predict deterministically. In particular, the effect of turbulence on the vortex strength is still little understood, thus the rate of motion along the trajectories (but not the trajectories themselves) cannot be precisely defined. Experimental data illuminating this point is presented later in Chapter 4.

Such problems will continue to reappear in the analyses which follow, and thus some ground rules concerning assumptions had to be established. In general it is assumed that:

- the wind is steady in time and is everywhere uniform
- the ambient turbulence is steady in time but may vary with height above the ground
- the vortex circulations remain constant and do not decay

3.2 Instability of a Wake Descending Near the Ground

As will be discussed later, it appears that generally (maybe always) the ultimate decay mechanism for a vortex is one of core breakdown. Empirical observations have indicated, however, that a slowly evolving mutual induction instability (a sinuous instability)

intervenes between vortex formation and this final catastrophic disintegration by core bursting, and sometimes reorders the vortex motion before the core breakdown occurs. The dynamics of the instability were studied by Crow (1970), who predicted the amplification rates of initially sinusoidal disturbances. Crow and Bate (1975) extended the theory to include excitation by atmospheric turbulence, but they restricted their analysis to altitudes large enough that the excitatory eddies lie in the Kolmogorov inertial subrange. Here the theory will be modified for more general turbulent input spectra, in order to handle situations near the ground where inertial subrange eddies are too fine to promote instability.

Following Crow (1970), define $y_1(x,t)$ and $y_2(x,t)$ as the lateral displacements of the port and starboard vortices from their undisturbed locations, according to the geometry displayed in Figure 3-2. Linking occurs when the difference quantity

$$y_s = y_1 - y_2 \tag{3.1}$$

in some locations equals the original vortex separation b_v, so that the vortex centerlines coincide there. If atmospheric turbulence is the source of disturbances, the $y_s(x,t)$ is random, and the easiest statistical quantity to handle is its mean square $\langle y_s^2 \rangle$. Crow and Bate define the lifespan T of the vortex wake by the prescription

$$\langle y_s^2 \rangle = b_v^2 \quad \text{at} \quad t = T \quad , \tag{3.2}$$

where y_s is to be calculated from linear stability theory. To allow the use of linear theory, the assumption is made that nonlinear effects which occur toward the end of the lifespan are important over a time short compared with the instability growth time T. The flight tests of this study, as well as previous experiments, suggest that this is indeed the case.

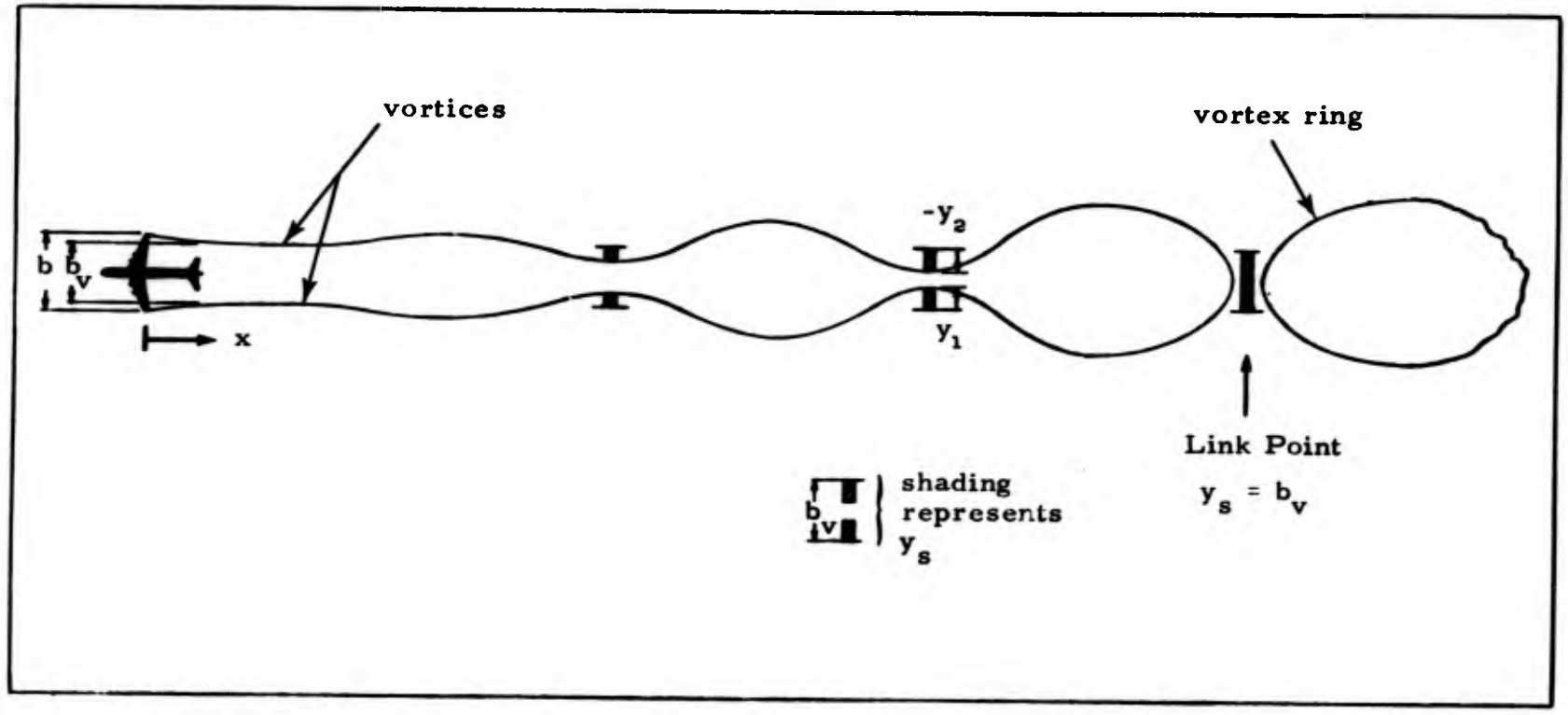

FIGURE 3-2. View of developing instability from above. The difference quantity, y_s, is represented, pictorially, by the shaded regions. The figure is not to scale.

It is convenient to express y_s as a Fourier integral,

$$y_s(x,t) = \int_{-\infty}^{\infty} y_s(k,t)\, e^{ikx}\, dk \quad , \tag{3.3}$$

and deal with individual Fourier modes $\hat{y}_s(k,t)$. When the wake altitude exceeds b_v , the vortex ground images can be neglected, and the differential equation for $\hat{y}_s$ derived by Crow and Bate can be applied directly:

$$\frac{\partial^2 \hat{y}_s}{\partial t^2} - a^2\, \hat{y}_s = \frac{2a\hat{w}}{\tan \theta_s} \quad , \tag{3.4}$$

where a(k) is either real or imaginary, depending on the wave number k . If a(k) is real, it can be interpreted as an exponential growth rate; if imaginary, its modulus is a frequency of oscillation. Tan $\theta_s(k)$ is a geometrical quantity that follows from the stability theory, and $\hat{w}(k,h)$ is the Fourier transform of the vertical component of turbulent velocity along the centerline of the wake. In the coordinates of Figure 3-2,

$$w(x,0,h) = \int_{-\infty}^{\infty} \hat{w}(k,h)\, e^{ikx}\, dk \quad , \tag{3.5}$$

where h is the wake altitude. Both $\hat{y}_s(k,t)$ and $\hat{w}(k,h)$ must be interpreted as generalized Fourier transforms, with correlations in wave number space proportional to delta functions. For example,

$$\langle \hat{w}(k,h)\, \hat{w}(k',h) \rangle = W(k,h)\, \delta(k+k') \quad , \tag{3.6}$$

which establishes a connection with the turbulence input spectrum W(k,h) discussed in Section 2-2.

Crow and Bate show that Eq. (3.4) should be solved in conjunction with the initial conditions

$$\hat{y}_s = 0 \quad , \quad \partial \hat{y}_s / \partial t = 0 \quad \text{at} \quad t = 0 \quad ,$$

to an accuracy consistent with the right-hand side of Eq. (3.4), and they show that the solution for real amplification rate a(k) is

$$\hat{y}_s = \frac{2\,\hat{w}}{a \tan \theta_s} \{\cosh (at) - 1\} \quad . \qquad (3.7)$$

The solutions for imaginary a(k) vary as the cosine rather than the hyperbolic cosine, but those modes do not amplify, and they make little contribution to $\langle y_s^2 \rangle$ at large times. Crow (1970) showed that real values of a(k) are largely confined to a wave number band $-k_o < k < k_o$ defined by a limiting wave number k_o inversely proportional to the vortex spacing b . A narrow band of unstable waves with wave numbers inversely proportional to vortex core diameter was dismissed as being unphysical, though the possibility of the short wave being real has since been raised (Widnall, 1974). As far as the mutual induction instability is concerned, in any event, we can concentrate on the band $-k_o < k < k_o$.

$\langle y_s^2 \rangle$ is obtained by integrating the product $\langle y_s(k,t)\, y_s(k',t) \rangle$ over all unstable wave numbers k and k′. From Eq. (3.6) and (3.7), then

$$\langle y_s^2 \rangle = 8 \int_0^{k_o} W(k,h) \left\{ \frac{\cosh [a(k)t] - 1}{a(k) \tan \theta_s(k)} \right\}^2 dk \quad . \qquad (3.8)$$

A factor of four comes from squaring the factor of two in Eq. (3.7), and an additional factor of two comes from restricting the integration

to positive values of k . An implicit formula for the lifespan T follows at once from the lifespan criterion, Eq. (3.2):

$$b_v^2 = 8\int_0^{k_o} W(k,h)\left\{\frac{\cosh\left[a(k)T\right]-1}{a(k)\tan\theta_s(k)}\right\}^2 dk \quad . \qquad (3.9)$$

Figure 3-3 shows the relationship between the amplification rate a(k) and the turbulence input spectrum W(k, h) for different wake altitudes h . From the previous discussion on atmospheric turbulence, Eqs. (2.10) and (2.14), W is independent of k for kh below about 3.

$$W = .58\ u_*^2 \quad , \quad k \lesssim 3h^{-1} \quad , \qquad (3.10)$$

and W varies as $k^{-5/3}$ for kh greater than about 5,

$$W = 0.593\ v_*^2 h^{-2/3} k^{-5/3} \quad , \quad k \gtrsim 5h^{-1} \quad . \qquad (3.11)$$

When h is large, the band of amplified waves lies entirely in the $k^{-5/3}$ inertial subrange (upper W curve in Figure 3-3), and the previous results of Crow and Bate are valid. As the vortex altitude h decreases, the input spectrum W(k, h) at first rises in the band of amplified waves (middle W curve in Figure 3-3). The bracketed amplification factor in Eq. (3.9) must fall to keep the value of that integral constant at b^2 , so the wake lifespan T must decrease as well. As h decreases further, the band of amplified waves embraces only the flat portion (Eq. 3.10) of the input spectrum (lower W curve in Figure 3-3). The relevant portion of W(k, h) decreases, and the lifespan T thus rises, but by that time interaction with the ground image has already become strong and other considerations come into play.

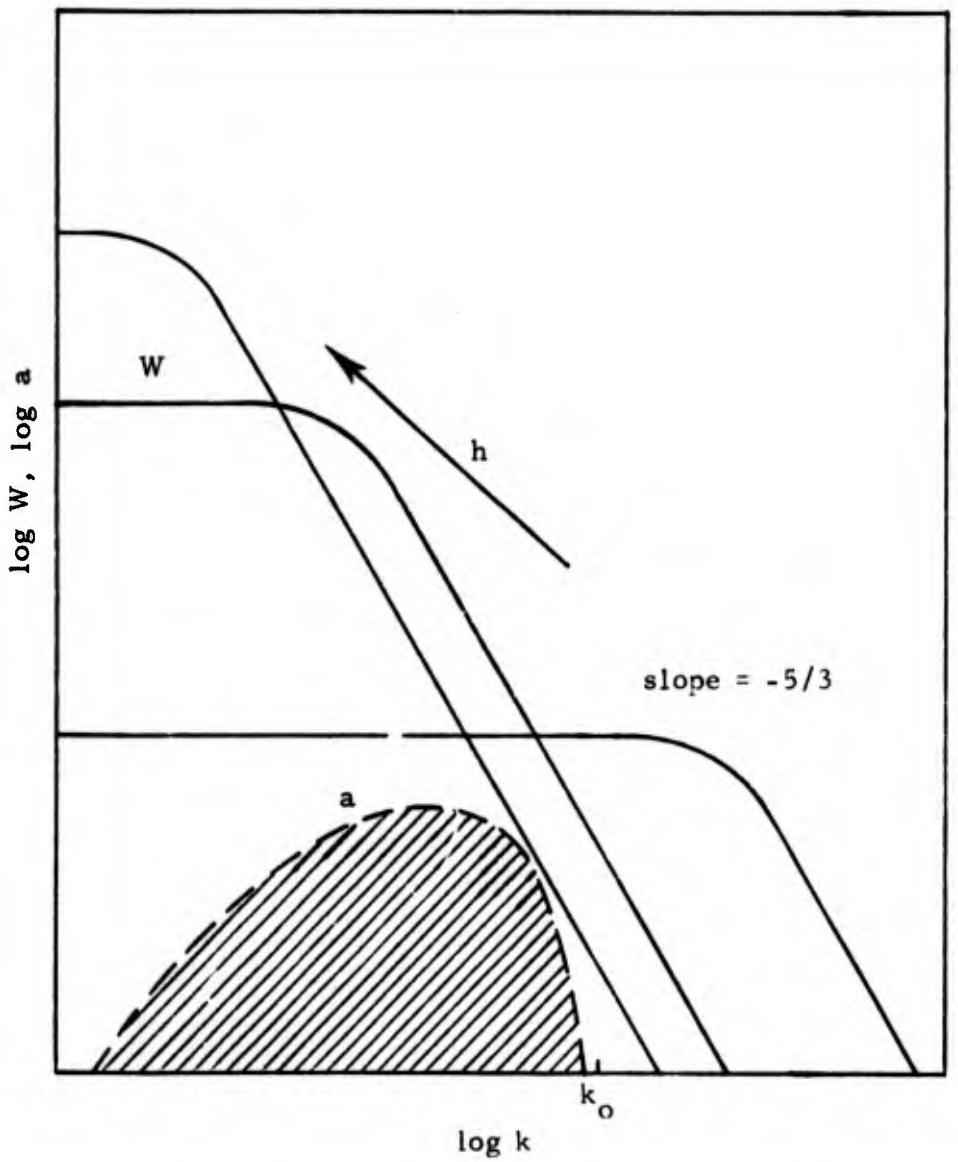

FIGURE 3-3. Overlap between amplification rate, a , and turbulence input, W , at various altitudes, h , in a constant stress boundary layer. The inertial subrange, which comprises -5/3, includes only the higher wavenumbers as the ground is approached. The band of amplified waves is marked by the shading.

It is advantageous to scale the physical quantities entering into Eq. (3.9) on the vortex circulation Γ and separation b :

$$k = \beta / b_v \quad , \tag{3.12}$$

$$a = \frac{\Gamma}{2\pi b_v^2} \alpha(\beta) \quad , \tag{3.13}$$

$$h = b_v \zeta \quad , \tag{3.14}$$

$$u^* = \frac{\Gamma}{2\pi b_v} \eta^* \quad , \tag{3.15}$$

$$W = \frac{\Gamma^2}{4\pi^2 b_v} \eta^* \zeta \mathcal{W}(\zeta\beta) \quad , \tag{3.16}$$

$$T = \frac{2\pi b_v^2}{\Gamma} \tau(\eta^*, \zeta) \quad . \tag{3.17}$$

The new parameters introduced have simple physical interpretation. β is the dimensionless wave number already used in Section 2.3 and α is the dimensionless amplification rate introduced by Crow (1970). ζ is the ratio of wake altitude to vortex spacing, and η^* is the ratio of turbulent friction velocity u* to vortex descent speed. Since turbulent boundary layer theory gives u* constant within a given boundary layer, η^* is also constant and characterizes the degree to which turbulence disturbes the vortices. In their analysis of the mutual induction stability for vortices excited by inertial subrange eddies, Crow and Bate used a turbulence intensity parameter η related to energy dissipation,

$$\eta = \frac{(\epsilon b_v)^{1/3}}{(\Gamma / 2\pi b_v)} \quad . \tag{3.18}$$

η is related to η^* through Eq. (2.8):

$$\eta = \frac{\eta^*}{(\kappa\zeta)^{1/3}} \quad . \tag{3.19}$$

(η would also be an acceptable measure of turbulence intensity, but unlike η^* it varies through the lower part of a wind-driven boundary layer). The dimensionless turbulence spectrum $\mathscr{W}(kh) = \mathscr{W}(\zeta\beta)$ was discussed thoroughly in Section 2.2. $\tau(\eta^*, \zeta)$ is a dimensionless wake lifespan, the ratio of the actual lifespan to the time required for the wake to descend a distance b .

With the substitutions of these dimensionless quantities, the lifespan equation, Eq. (3.9), takes the form

$$\frac{1}{\eta^{*2}} = 8\zeta \int_0^{\beta_o} \mathscr{W}(\zeta\beta) \left\{ \frac{\cosh\left[\tau\alpha(\beta)\right] - 1}{\alpha(\beta) \tan\theta_s(\beta)} \right\}^2 d\beta \quad . \tag{3.20}$$

The quantities $\alpha(\beta)$ and $\alpha(\beta) \tan\theta_s(\beta)$ can be computed from Crow's original paper and are plotted in Figure 3-4. $\alpha(\beta)$ vanishes at

$$\beta_o = 1.12 \quad , \tag{3.21}$$

which serves as the upper limit for the integral in Eq. (3.20). Our procedure is to integrate Eq. (3.20) numerically, using tabulations of the curves in Figure 3-4 and the input spectrum, Eq. (2.14), obtained from meteorological considerations. The integrations yield η^* as a function of τ and ζ , and the results are finally plotted as a two-parameter family of dimensionless wake lifespans $\tau(\eta^*, \zeta)$. The results are presented in Figure 3-7, which will be discussed in the next section after corresponding results have been derived for the case of strong ground effect.

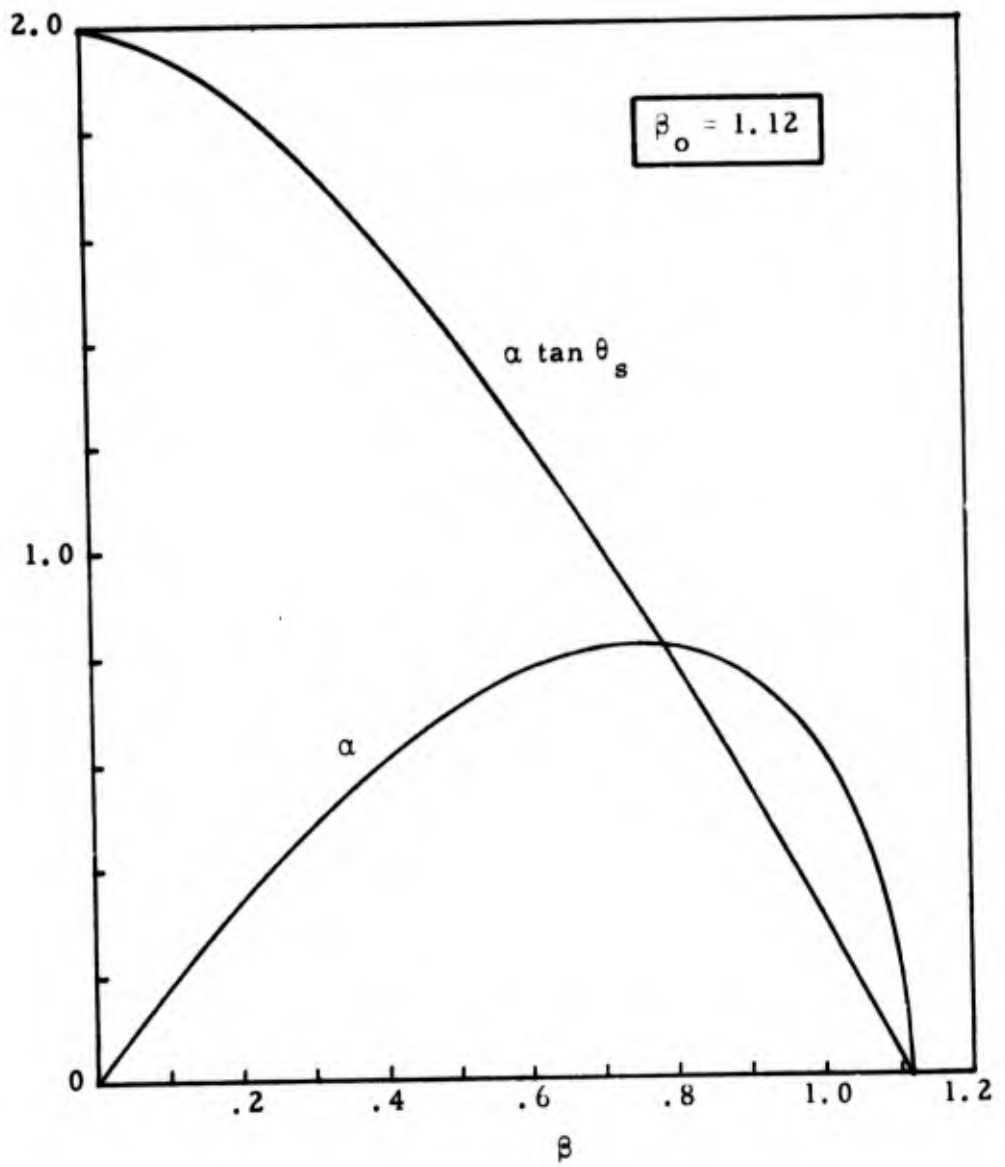

FIGURE 3-4. Various quantities involved in the vortex dynamics as functions of the dimensionless wavenumber, β.

3.3 Lifespan of a Vortex Interacting Strongly with Its Ground Image

So far the presence of the ground has been considered only insofar as it affects the turbulent input spectrum. As the vortex wake descends to within a distance b of the ground, however, the ground effect begins to alter the dynamics of the vortices themselves. The vortices interact strongly with their ground images, and for a short time the flow can be described in terms of four interacting vortices. The unperturbed flow is non-steady in all coordinate systems, and the simple notions of exponential instability do not apply. This state lasts for a time of order $2\pi b_v^2/\Gamma$ (about 7 seconds for a 747), after which the original vortices will have separated enough so that each may be treated in isolation with its image, with which each travels laterally at a height $h = b_v/2$, as described in Section 3.1.

Figure 3-5 illustrates the geometry of the mutual induction instability after the real vortices have separated. The mutual induction instability is symmetric, so the image interacts with the real vortex just as though the image were the second element of a vortex pair. When the real vortex links with its image, the result is the croquet-hoop formations reported by Bisgood, Maltby, and Dee (1971) and observed in the present tests.

The mutual induction instability thus evolves as before, the only change being that x-y supplants x-z as the plane of symmetry for the interaction. Thus, the analysis of the instability follows Section 3.2 without change, except that $v(x, y, b_v/2)$ replaces $w(x, 0, h)$ as the dominant component of turbulent convection velocity. In place of the lifespan formula of Eq. (3.9), there is now the relation

$$b_v^2 = 8 \int_0^{k_o} V(k, b_v/2) \left\{ \frac{\cosh\left[a(k)T\right] - 1}{a(k) \tan \theta_s(k)} \right\}^2 dk \quad , \qquad (3.21)$$

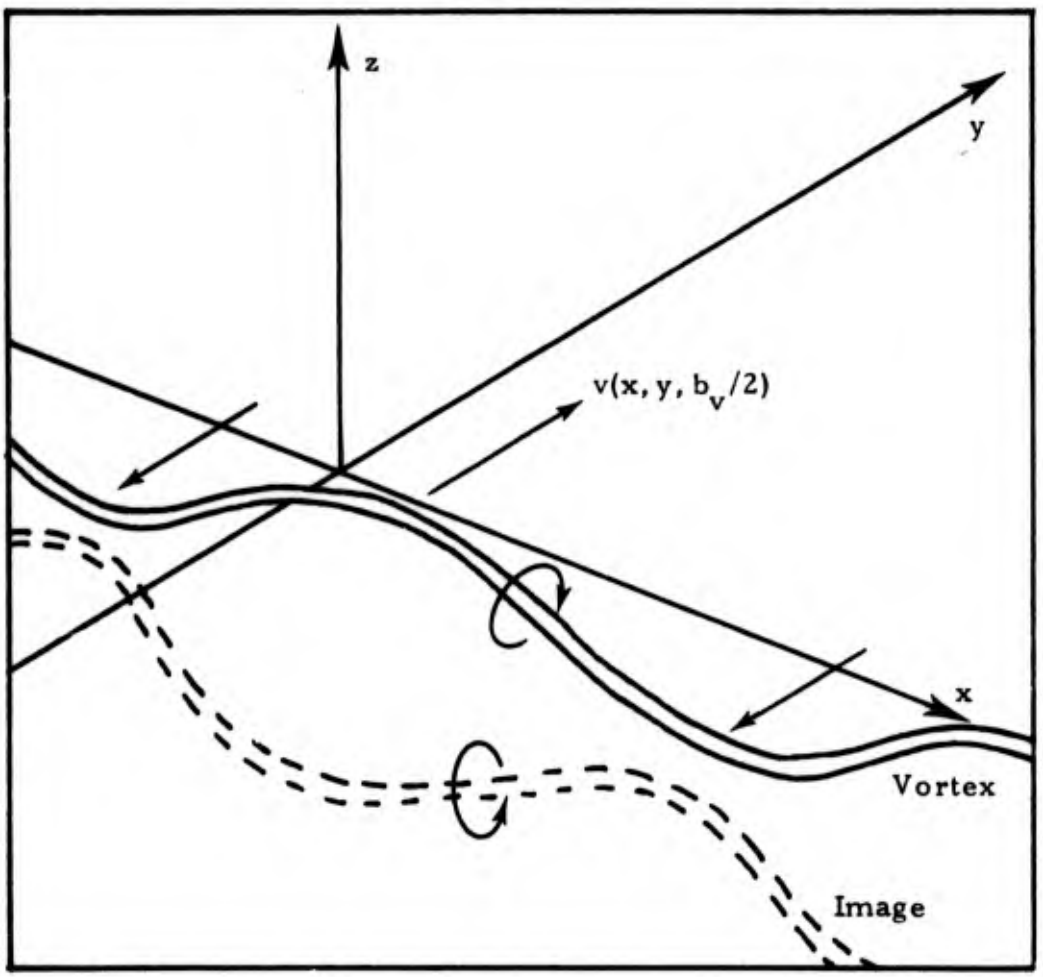

FIGURE 3-5. Interaction between a vortex and its ground image after the vortex has separated from its original companion.

where $V(k, b_v/2)$ is the spectrum of the windward component of turbulence which was discussed in Section 2.3. Under the scaling assumptions, Equations (2.18) and (3.12) through (3.17), the equation governing lifespan in full ground effect becomes

$$\frac{1}{\eta^{*2}} = 8 \int_0^{\beta_o} \gamma'(\beta) \left\{ \frac{\cosh [\tau \alpha(\beta)] - 1}{\alpha(\beta) \tan \theta_s(\beta)} \right\}^2 d\beta \quad . \qquad (3.22)$$

Again $\alpha(\beta)$ and $\alpha(\beta) \tan \theta_s(\beta)$ are to be taken from Figure 3-4, and $\gamma'(\beta)$ is the dimensionless spectrum plotted in Figure 2-3, which has been replotted in Figure 3-6 together with the dimensionless amplification rate. $\gamma'(\beta)$ can be approximated by the quadratic

$$\gamma'(\beta) \approx 0.38 + 0.15\beta^2 \qquad (3.23)$$

over the range $0 < \beta < 1.12$ where $\alpha(\beta)$ is non-zero. This form was used in the numerical integration of Eq. (3.22).

In Section 3.2, τ emerged as a function of dimensionless turbulence intensity η^* and vortex altitude ζ, whereas the τ in Eq. (3.22) is a function of η^* only because the dimensionless altitude ζ has been fixed at $h/b_v = 1/2$. Taken together, Equations (3.20) and (3.22) define a two-parameter lifespan function $\tau(\eta^*, \zeta)$, with Eq. (3.20) being appropriate for $\zeta \tilde{>} 1$ and (3.22) for $\zeta = 1/2$. Figure 3-7 shows lifespan functions calculated on that basis for $\zeta = 25$, 5, 1, and 1/2. The theory of Crow and Bate (1975) should be used for $h/b_v = \zeta \tilde{>} 10$ (for the class of aircraft used in the experimental portion of this program, with $b_v \approx 10$ m), since the scaling laws appropriate for the constant-stress region of the atmospheric boundary layer will break down at altitudes h greater than, typically, about 100 meters (as was discussed in Section 2.1), and can have applicability over an even smaller range of altitudes in very stable conditions.

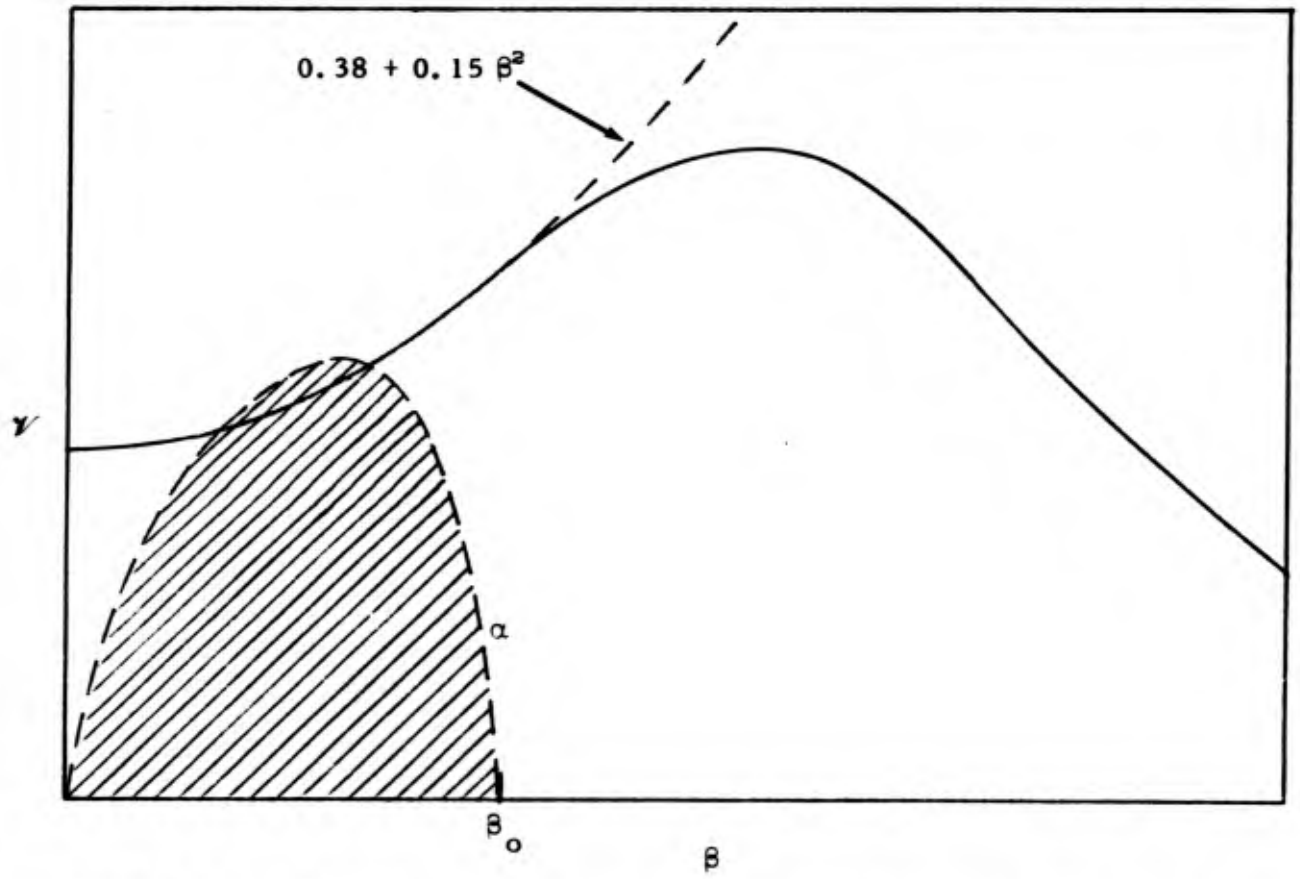

FIGURE 3-6. Comparison between the dimensionless input spectrum, $\gamma(\beta)$, and the amplification rate, $\alpha(\beta)$, for a vortex in ground effect.

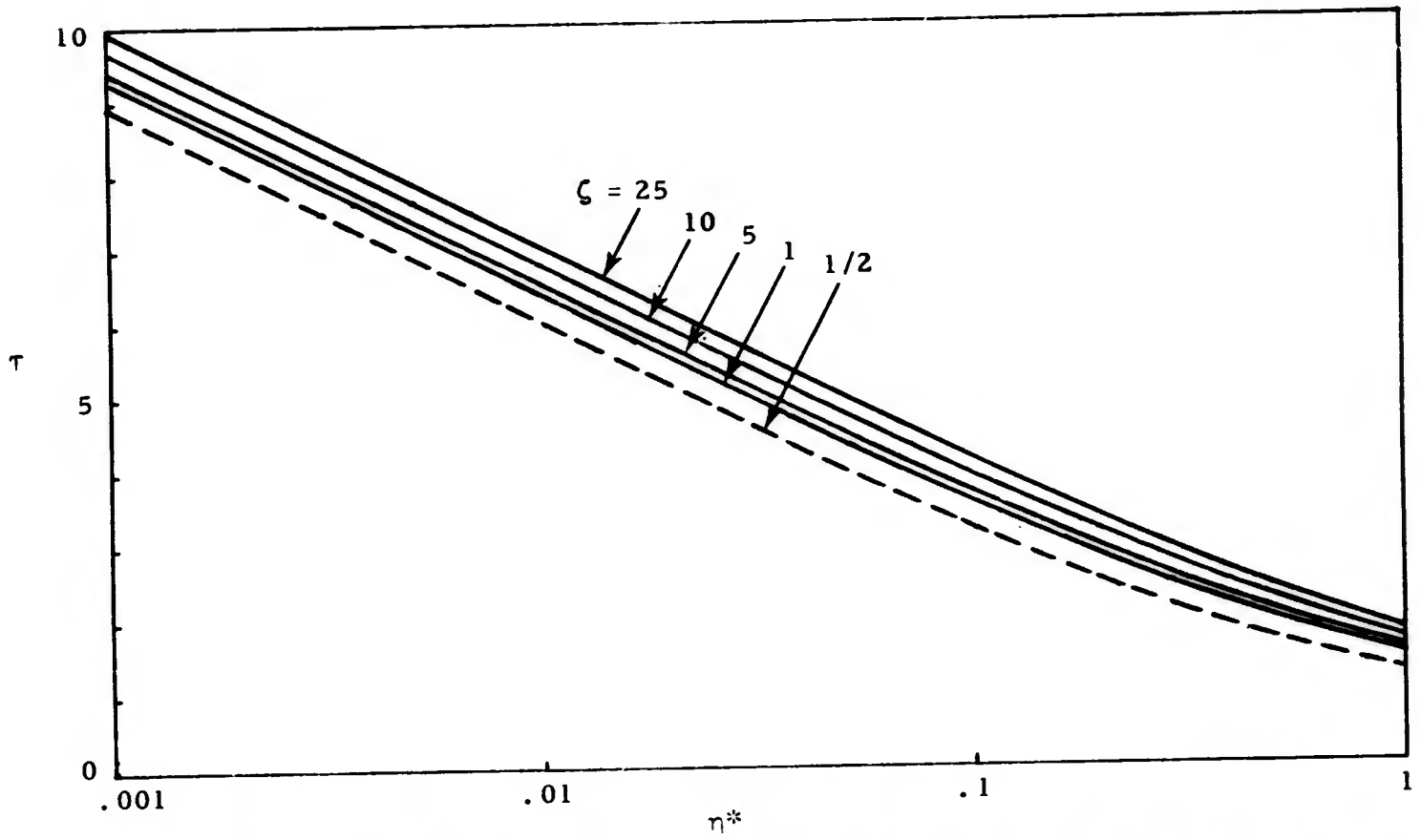

FIGURE 3-7. Dimensionless wake lifespan as a function of $\eta^* = v^*/(\Gamma/2\pi b)$ and $\zeta = h/b$. The solid lines were computed using the theory of Section 3.2, for which the altitude variation of the turbulent forcing function was considered, while the dashed curve is based on the analysis of this section where the interaction occurs between the vortex and its image.

The overriding conclusion to be drawn from Figure 3-7 is that wake lifespan is relatively insensitive (order of 10%) to altitude. At fixed η^* (recall that η^* is constant in the lower part of the boundary layer), the lifespan shortens as the wake descends from 25 b_v to about b_v . The lifespan shortens further as the wake enters ground effect and the image vortices enter the equation, and the minimum lifespan is reached at $h/b_v = 1/2$. These conclusions agree at least qualitatively with the flight test results, though it must be emphasized that the lifespans predicted here depend on the intervention of the mutual induction instability. During the experimental program core bursting was often observed prior to instability and linking, but the curves of Figure 3-7 should always be valid upper limits on the lifespan of wakes near the ground.

4. EXPERIMENTS ON WAKE

4.1 Description of Experimental Program

Experiments were conducted on two consecutive test days, 11-12 February 1975, at El Mirage Dry Lake in the Mojave Desert, California. Advantage was taken of the calm, stable conditions which often exist in the Mojave Desert in winter during the early morning hours. For this reason the tests were performed after sunrise, as soon as there was sufficient light for photography, and continued until solar heating had deteriorated the desired calm meteorological conditions -- usually by about 11:00 a.m.

Generator Aircraft

The test aircraft used was an Aero Commander 560A light twin-engine airplane. Three groups of three each Army M-18 smoke grenades were mounted on each wingtip to make the vortices visible by the injection of smoke. Two different colors of smoke, red and green, were used to identify the left and right vortices, respectively. Figure 4-1 shows the smoke grenades mounted on the left wingtip of the Aero Commander.

The Aero Commander was also used to fly meteorological soundings between test runs and to obtain turbulence data during the test runs themselves. Information obtained from the soundings included temperature and turbulence profiles as a function of altitude above the test site. Figure 4-2 shows the pitot probe used to obtain the turbulence data mounted on the nose of the aircraft.

Table 4-1 lists the flight parameters associated with the test airplane which were important in characterizing its wake structure.

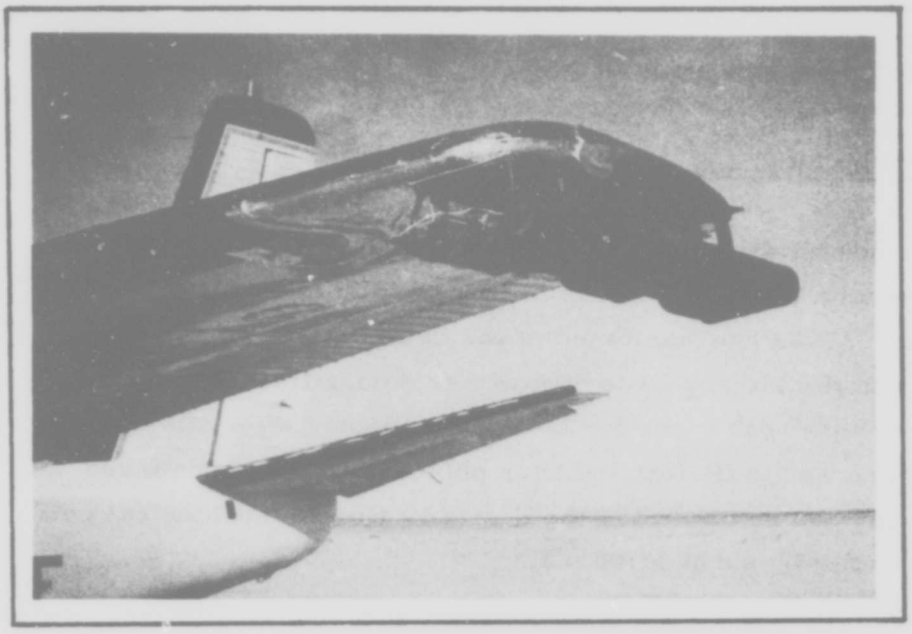

FIGURE 4-1. View of the left wingtip of the Aero Commander, showing the installation of the smoke grenades.

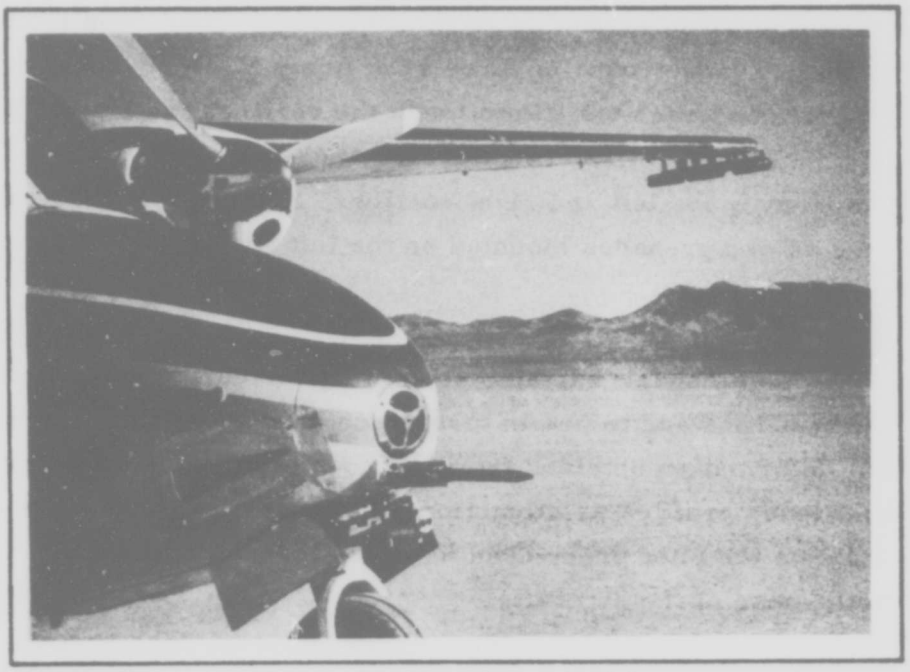

FIGURE 4-2. The test aircraft parked between runs for replacement of grenades. The pitot static probe for turbulence measurement can be seen on the nose of the aircraft. The smoke grenades shown in Figure 4-1 are also visible.

TABLE 4-1. Flight parameters of Aero Commander 560A.

Mass, W	2636 kg
Wingspan, b	13.5 m
Airspeed (true, average), U	49 m/sec
Vortex spacing (elliptic loading), b_{ve}	10.6 m
Circulation (elliptic loading), Γ_e	40.6 m^2/sec

Test Site

The test site consisted of a section of the flat lake bed at El Mirage Dry Lake. This particular area was selected to provide a straight, level, continuous run near the ground at the desired heading (all runs were flown at 250°) which was clear of obstacles. Figure 4-3 is an overhead view of the test site showing the Aero Commander with the smoke streaming from its wingtips. The fiduciary was marked on the desert floor with white chalk as a scale reference for overhead photography. Flags mounted on tripods at each end of the chalk marker provided the same scale reference for ground-based photography. The length of the chalk mark in the flight path direction is 100 feet.

Data Acquisition

Data associated with the geometry of the Aero Commander vortices was obtained photographically. A Hughes 269A helicopter hovering typically 400 m overhead provided a stable platform for vertical photography, and a ground-based site some 400 m to the side of the flight path provided views of the developing wake in the vertical plane. Table 4-2 lists the photographic equipment used at both the air and ground-based camera stations.

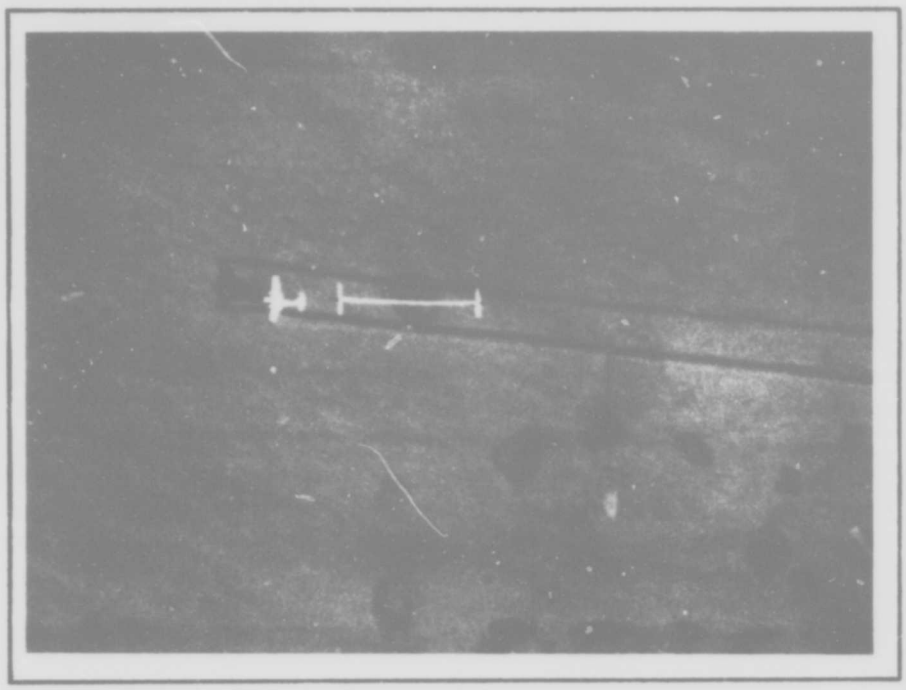

FIGURE 4-3. Overhead view of the test site from the helicopter. The chalk mark is 100 feet in the flight path direction. The shadows of the vortices are more pronounced than the vortices themselves. Beginning of Run 4. The crosswind from the right (top of the figure) is evident.

TABLE 4-2. Photographic equipment.

Site	Camera	Type	Lens	Framing Rate
Air	Nikon F	35 mm still	50 mm	1 fr/ 5 sec
Ground	Nikon F	35 mm still	50 mm	1 fr/5 sec
Ground	Arriflex 16S	16 mm cine	25 mm	16 fr/sec
Ground	Kodak Retina III Reflex	35 mm still	50 and 135 mm	--

Meteorological data associated with the upper atmosphere was obtained by using the Aero Commander as a sounding aircraft. Surface conditions were obtained from instrumented 4-meter meteorological towers at the locations of the test site and the ground camera station.

Wind direction and velocity and ambient temperature were measured at the ground camera station on both test days. In addition, the vertical wind w and its r.m.s. variation σ_w, and the cross-wind v and its r.m.s. variation σ_v were also measured there on the first day. On the second day this latter instrumentation was moved to a location adjacent to the flight path. On both days, an additional instrument for measuring v and σ_v was located at the test site. Figures 4-4 and 4-5 show the instrumentation at the camera station and that located at the test site.

Operations

Runs were made over the test site by the Aero Commander vortex generator at various altitudes between 8 and 34 meters. Actual determinations of altitude were made during data analysis of the side view photographs by observing the position of the airplane relative to a calibrated scale in view of the cameras. Three such runs were made consecutively and then the aircraft had to land for replacement of smoke grenades. Fifteen runs were made on each of the two test days, for a total of 30 runs. In addition to the low-level runs, four runs were made at altitudes above 100 m to provide a baseline for correlation of data from this program with that from previous work.

During passage of the airplane, its path and the subsequent evolution of the wake in the area of the test site were photographed from the ground and overhead. The time base for all of the ground-

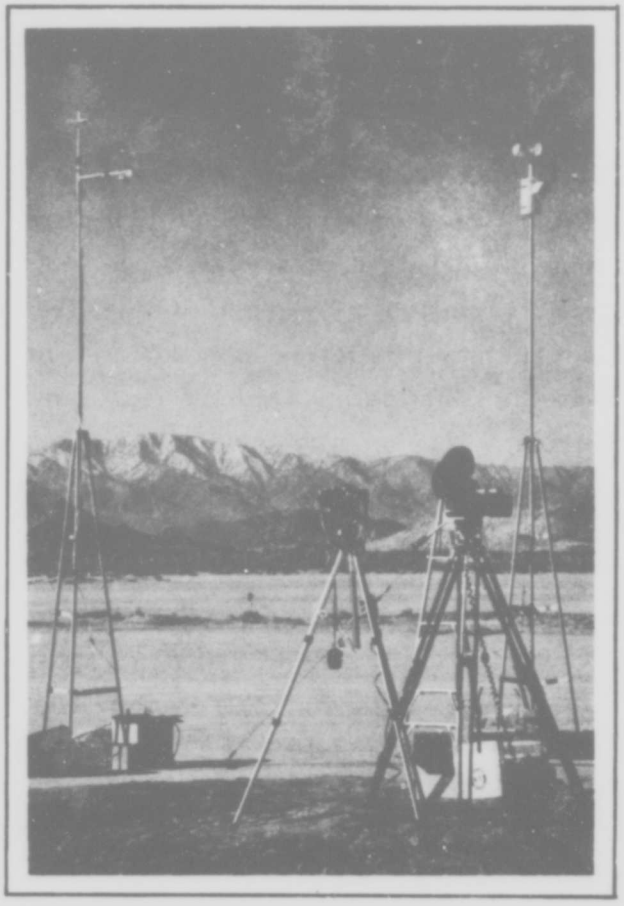

FIGURE 4-4. View of the test instrumentation at the ground station. Both the 35 mm still and 16 mm cine cameras are shown, as well as the meteorological towers.

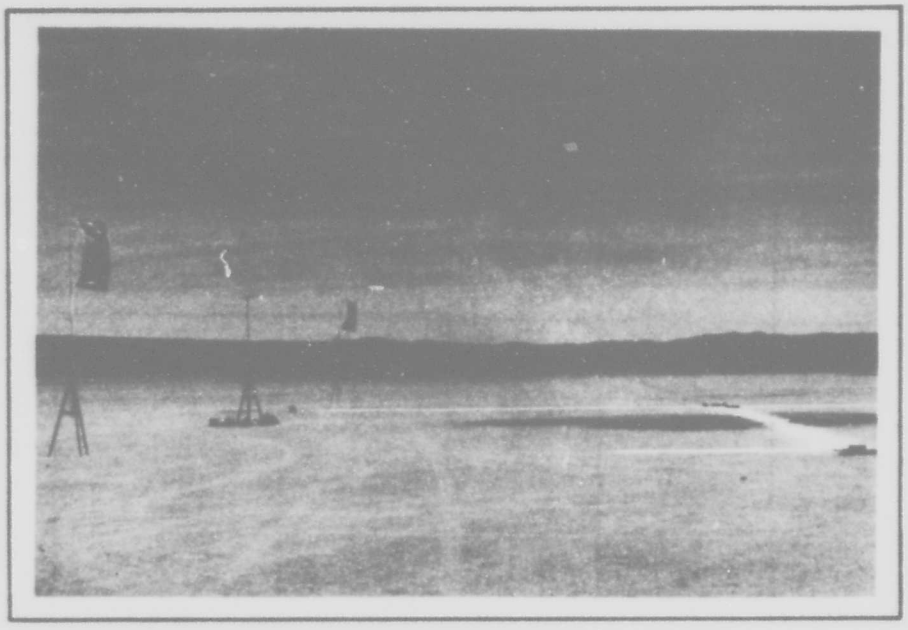

FIGURE 4-5. Equipment at test site, showing the scale reference flags, meteorological tower, and chalk marker. View is along flight path.

based photographic data was a clock with a sweep second hand in the field of view of the cameras, and additionally the framing rates of the cameras themselves. The overhead photographic data relied upon the framing rate of the camera for a time base.

Table 4-3 is a catalog of the experimentally measured test conditions for each of the runs made during this test program.

4.2 Discussion of Results

Vortex Spacing Aloft

Two separate runs, numbers 29 and 30, gave excellent time histories of the separation of the vortex pair out of ground effect.

TABLE 4-3. Atmospheric conditions near the position of the test site for each run.†

Run	Turbulence $\epsilon^{1/3}$ ($cm^{2/3} sec^{-1}$)	Temp (°C)	Lapse Rate γ (°C/100m)	Wind Speed (ms^{-1})	Wind ** Direction (degrees)	Crosswind (+) from right (ms^{-1})	Flight Altitude (m)
1	.5	-0.1	4.6	0.4	230	-0.1	8
2	.6	-0.3	4.6	0.4	230	-0.1	5
3	.6	-0.1	4.6	0.4	230	-0.1	5
4	1.0	2.7	5.9	0.5	0	+0.5	5
5	1.0	2.7	5.9	0.5	0	+0.5	9
6	0.8	1.9	5.9	0.5	0	+0.5	8
7	1.2	6.0	0.2	0.2	60	0	7
8	0.9	5.6	0.2	0.2	60	0	10
9	1.4	6.3	0.2	0.2	60	0	7
10	1.3	6.8	-1.0	0.4	270	+0.1	11
11	1.5	6.8	-1.0	0.4	270	+0.1	16
12	1.6	6.8	-1.0	0.4	270	+0.1	14
13	2.0	8.3	-1.1	0.6	270	+0.2	17
14	1.4	7.8	-0.2	-	-	-	123*
15	1.3	7.8	-0.2	-	-	-	123*
16	0.2	1.7	6.9	0.3	120	-0.2	4
17	0.3	1.2	6.9	0.3	120	-0.2	4
18	0.3	0.9	6.9	0.3	120	-0.2	4
19	0.8	2.4	5.1	0.4	280	+0.2	9
20	0.8	2.4	5.1	0.4	280	+0.2	8*
21	0.8	2.4	5.1	0.4	280	+0.2	11*
22	1.1	3.9	0.5	0.3	30	+0.2	11*
23	1.2	4.8	0.5	0.3	30	+0.2	11*
24	1.3	4.8	0.5	0.3	30	+0.2	15*
25	1.1	6.8	0.2	-	-	-	30
26	1.4	6.8	0.2	-	-	-	33
27	1.3	6.8	0.2	-	-	-	34
28	1.1	9.2	-0.3	-	-	-	30
29	0.3	10.3	1.6	-	-	-	213*
30	0.4	10.8	1.0	-	-	-	213*

† Temperature, turbulence, and lapse rate determined at point of closest approach of sounding aircraft to ground -- about 8 m for most runs.

* Obtained from run scenario; not determined photogrammetrically

**Aircraft heading = 250° for all runs

- Data missing or not obtained

Figure 4-6 shows the Aero Commander flying into view in the first sequence photo of Run 29. The view is from the ground camera station looking vertically upward. Figure 4-7 shows the results of a closer examination of the remainder of the photo sequences for the same two runs. Such data is of particular interest to establish the wake-aloft characteristics for the Aero Commander 560A for comparison with the 560F used during previous experiments (Tombach, 1974; Tombach, Bate, and MacCready, 1974) in order to verify the validity of comparison of results obtained with these slightly different aircraft.

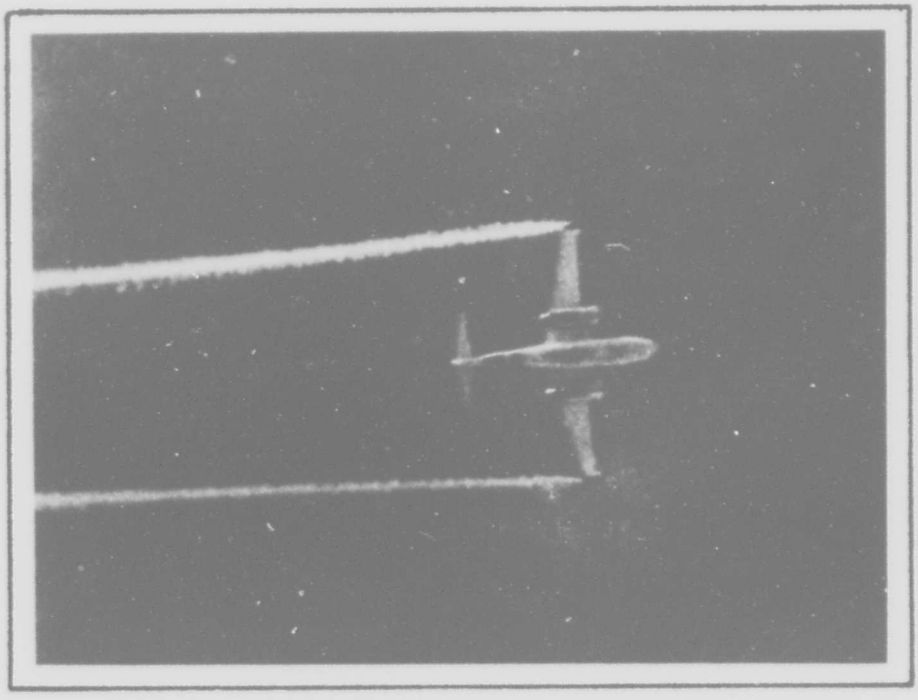

FIGURE 4-6. High altitude test run (altitude 213 m). View from ground camera station at the beginning of Run 29.

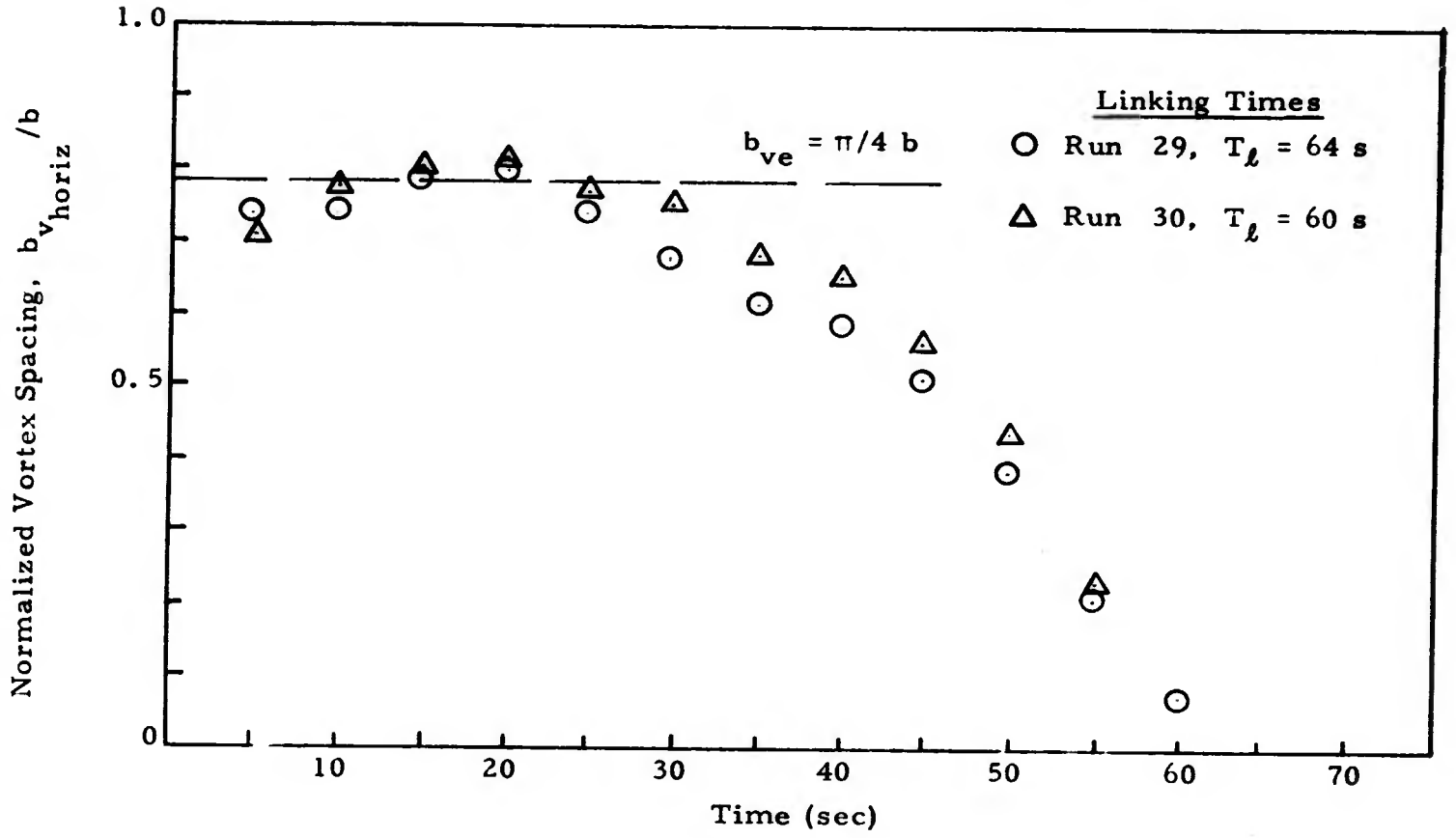

FIGURE 4-7. Horizontal vortex spacing aloft for Aero Commander 560A. The vortex spacing for elliptical wing loading for this aircraft is also shown. The decrease in spacing after 20 seconds is due to wake tilting.

Figure 4-7 shows the horizontal vortex spacing at a single fixed station on the photos, which were taken at 5-second intervals. For our purposes here the first 20 seconds are of greatest interest in establishing the wake characteristics of the 560A. The initial spacing, just after vortex generation, is about 0.7 b, or about 0.9 b_{ve}. This is somewhat larger than the 0.78 b_{ve} value observed for the 560F, and corresponds more closely to an elliptic lift distribution. The spreading of the vortices initially (for the first 15 seconds) occurs at a rate of about 0.4 b_{ve} per minute, which is about 10 times the rate observed for the first minute of 560F wake spreading. This difference is surprising, but cannot be viewed as a general characteristic based on data obtained from only these two runs.

The rapid decrease in apparent vortex spacing which appears after 20 seconds is caused by tilting of the wake (see Tombach, et. al., 1974, for a discussion); the data in Figure 4-7 shows only the horizontal projection of the vortex spacing. The photographic records show the wake had tilted 90° at about 60 seconds of age. Assuming a constant rate of roll of 90° per minute, one can then roughly compute the actual vortex spacing. This is shown in Figure 4-8 for the first 50 seconds. Errors in the computation procedure make data unreliable after that time. The main point of this figure is to show that the actual vortex spacing can increase substantially whenever the wake becomes non-horizontal, which has also been observed in previous work (Tombach, 1973).

It is probable that, from the standpoint of vortex kinematics, the two wakes produced by the 560A and 560F models of the Aero Commander are indistinguishable from each other immediately after generation, with the small differences noted above. The rapid increase in vortex spacing for these tests is not easily explained, however, and insufficient data was collected to draw firm conclusions about it.

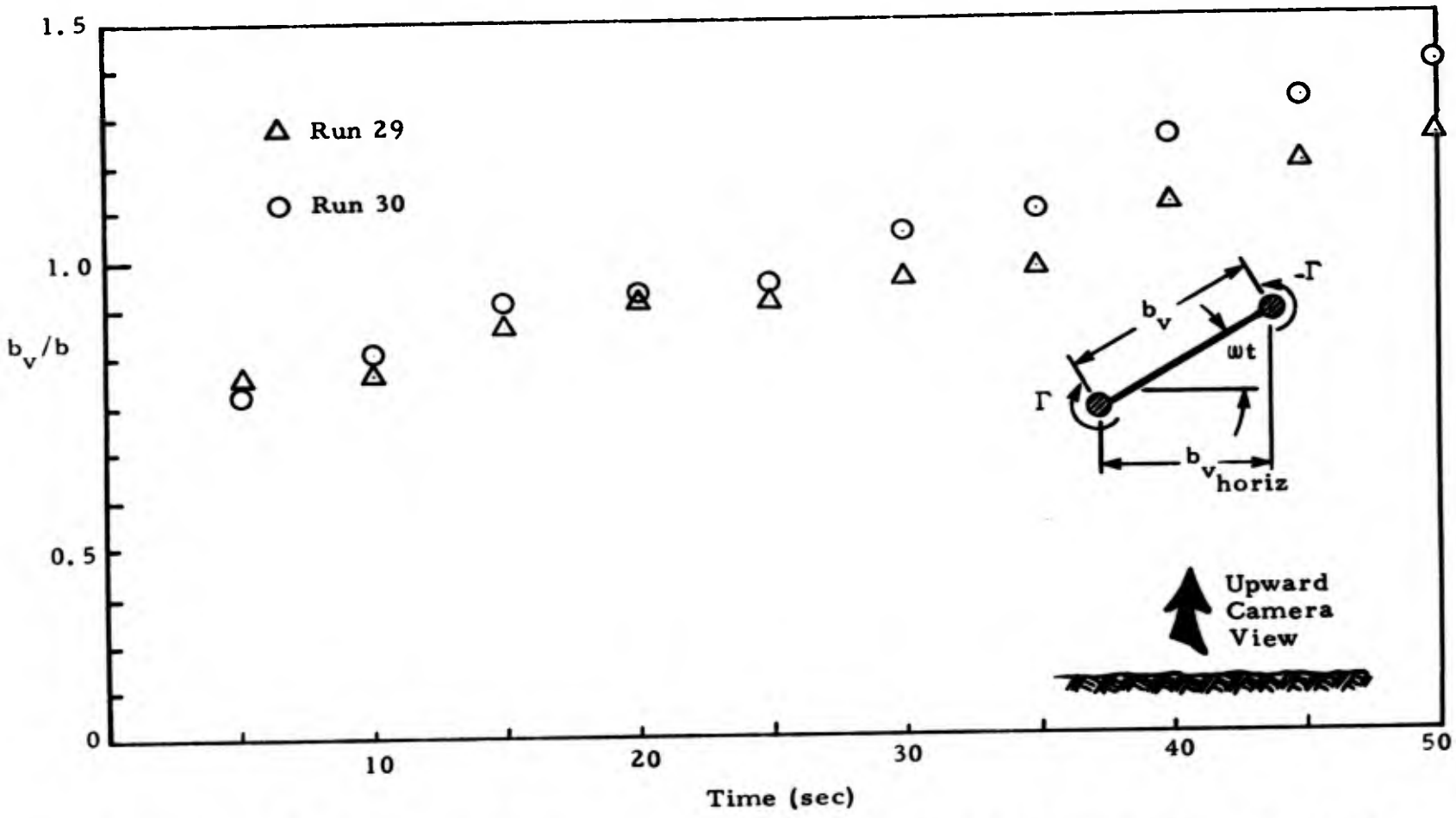

FIGURE 4-8. Approximate calculated vortex separation for the tilting wakes of Figure 4-7, based on an assumed constant wake roll rate ω of 1.5°/s.

Vortex Separation Trajectories Near Ground

A discussion of computed vortex trajectories in ground effect as a function of generation altitude was presented previously in Section 3.1. Here our concern is measurements of the horizontal projection of actual trajectories, which result in the spreading of the vortex pair as it descends toward the ground.

The aerial helicopter platform provided an excellent means of obtaining photographic data from above, by looking down at the developing wake motions. Data on the spreading of the vortex pair is presented along with analytical results in Figure 4-9. Again, here, the continuous nature of the photographic data gives a very reasonable "picture" of the developing wake motion. However, the data for each of the generation altitudes presented in Figure 4-9 were averaged over several runs flown at equivalent altitudes, so that the individuality associated with a specific run has been lost (except for the 30 m generation altitude, where only one run is included and the oscillatory behavior of the vortex separation, associated with the Crow instability, is clearly present).

The pattern of motion is quite consistent, regardless of generation altitude. In all cases the experimentally measured data agree with the theoretically computed separation trajectory until the vortices are 25-30 m apart. Examination of Figure 3-1, showing the analytically derived descent trajectories, reveal that at such a separation (approximately 2.5 b_{ve}) the vortices have in all cases completed their descent and are traveling laterally. Beyond this separation Figure 4-9 shows a perceptible slowing down of the rate of vortex separation, with separation speeds at 35 m spacing about half those at 20 m. In those cases where vortex persistence allowed further measurements, the separation rate had decreased to a virtual standstill after a 40 m separation had been attained.

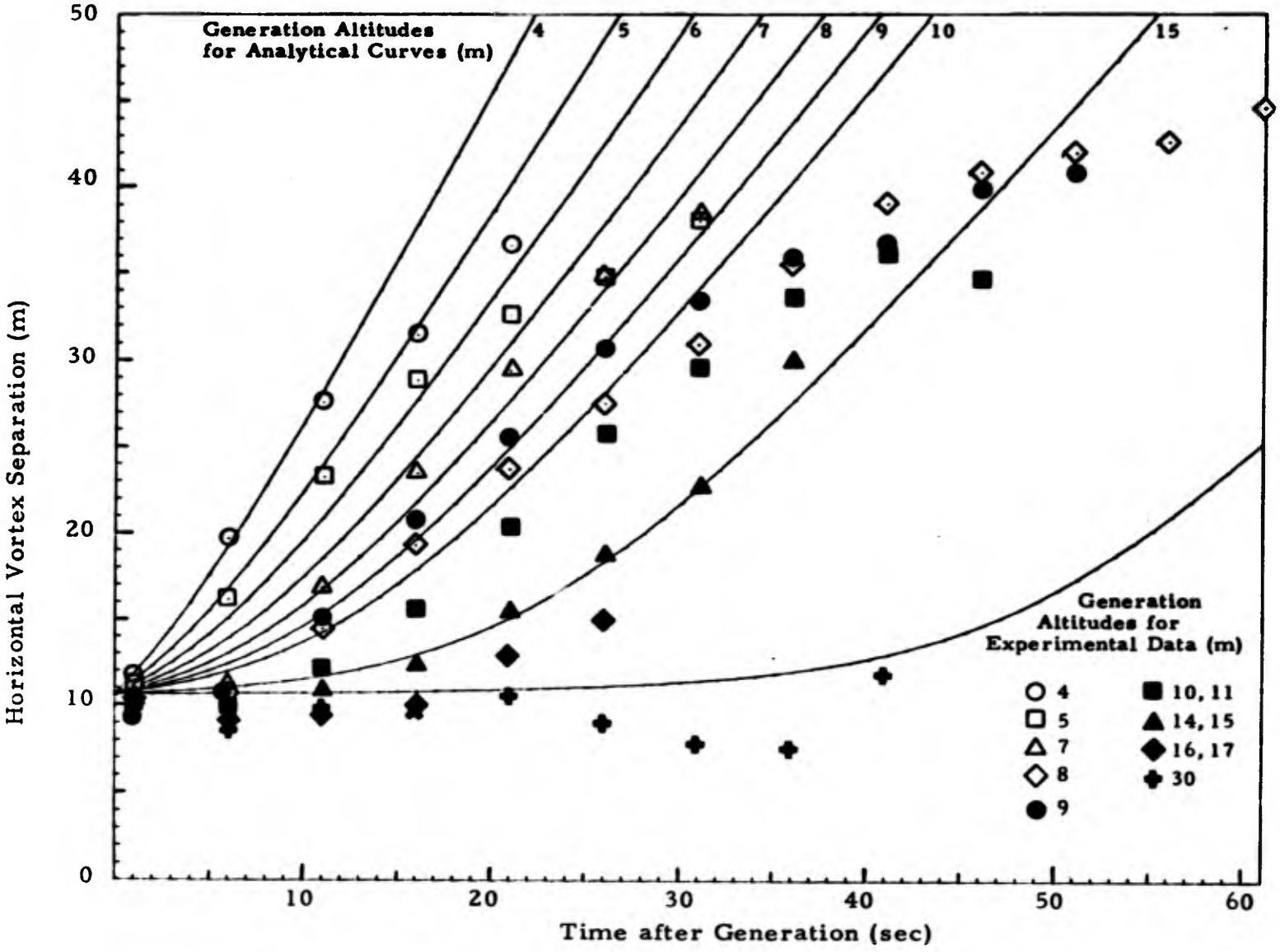

FIGURE 4-9. Horizontal spreading of vortex pair in ground effect as a function of generation height above ground.

These observations, which are relatively independent of the original generation height of the vortices, and which do not reflect any obvious systematic effects of wake age, do not correspond with the common view of a simple separation of vortices at constant speed. Rather, the slowing of separation probably indicates a slow erosion of vortex strength by diffusion of the vorticity generated at the ground interface between the "cells" of the real and image vortices. This behavior differs from that for a descending vortex pair where the dividing streamline between the two vortex cells has no stress across it, and thus does not generally exert a dissipatory influence on the vortex circulations.

For completeness, an alternative explanation for the observed behavior could be a rising of one or both of the vortices, which would thereby decreases the speed of separation. The experimental data show this to occur occasionally, especially when vortices are generated quite close to the ground. Otherwise, rising does not appear to be occurring to any significant degree, and thus the erosion of strength is a more likely explanation. The effects of vorticity generation at the ground surface should be most pronounced when a vortex is traveling very close to the ground. The data in Figure 4-9 show, indeed, that the separation rate slows down at an earlier time for the vortices generated at low altitudes than it does for the vortices generated at higher altitudes. Thus, the slowing, which occurs at about the same separations and to the same degree regardless of generation altitude, has to be effected in a shorter time by a stronger influence for the low-level vortices than for those generated and remaining more aloft.

Vortex Decay

For all of the experimental runs near the ground, the vortices were ultimately destroyed by breakdown, initiated either by core bursting or linking followed by core bursting. This study was initially

conceived to examine the effects of the ground on the linking phenomenon. However, since both instabilities were routinely observed, and since wake lifetime is a composite of the effects of both, a discussion of the experimental observations of both types of wake instabilities is presented here.

All of the times at which the instabilities occurred were obtained from the photographic records taken during the experimental program. Core bursting was relatively easy to distinguish using the aerial photographs. The linking phenomenon was somewhat more difficult to identify and the ground-based movies supplied most of the information on link times because linking near the ground always occurred between the vortex and its image. Thus, the classic picture of the vortex pair moving together and ultimately contacting (as happens at altitude) was not what was seen in ground effect. More than likely, many more link situations were recorded by the various photographic methods than are presented here as data points, but it was not possible to definitively identify them as such because of the lighting or background of the pictures.

Figure 4-10 summarizes the measured times for the observed instabilities as a function of the atmospheric turbulence level in the test area. Also shown on the figure is the theory of Crow and Bate (1975) for linking times out of ground effect as well as the modified theory in heavy ground effect, where linking is with the image, from Section 3.3 of this report. These curves were obtained using the aircraft parameters for the Aero Commander 560A (listed in Table 4-3) as inputs to the theory, using Eqs. (3.18) and (3.19) to relate η^* and ϵ for calculating the theoretical curves.

Links. Figure 4-10 shows the links that were observed at 30 m and above and those below 30 m. For the higher altitude cases, the agreement of the data with the theory of Crow and Bate is quite good. A graphical representation of a mean fit to this data has not

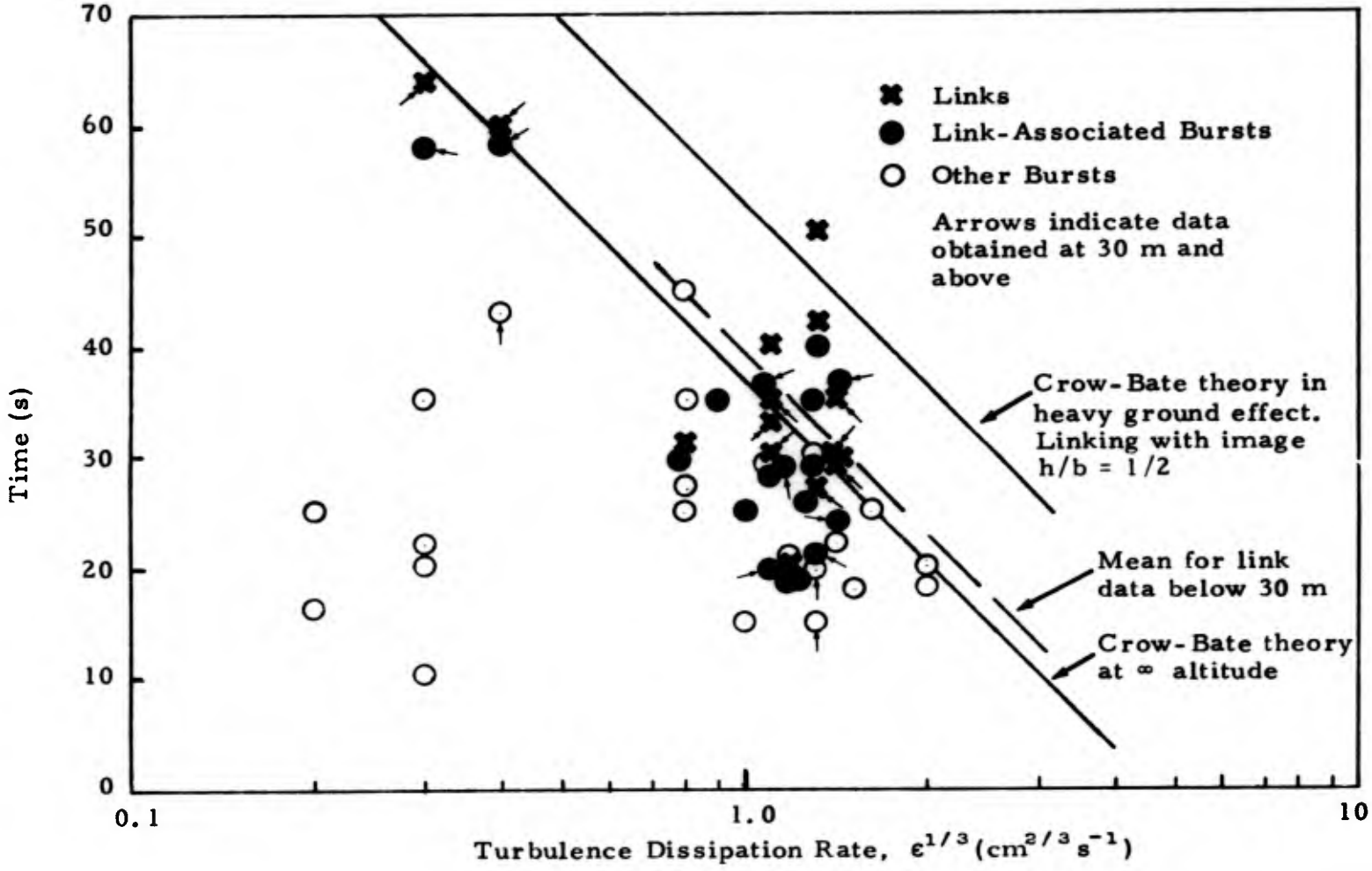

FIGURE 4-10. Vortex destruction due to instabilities both in and out of ground effect. Aero Commander 560A aircraft. Core bursts on linked vortex loops are not shown.

been drawn on the figure because, by inspection, it would not differ much from the theory for "infinite" altitude.

However, the data scatter for the cases below 30 m is sufficiently great that a line representing the mean of the data is helpful, and is included as a dashed line on the figure. This line was drawn such that it had the same slope as the theory so that the mean time error $\Sigma \Delta t_j$ was zero, where Δt represents the time deviation of each data point from this mean line. Since the data points were obtained for a range in generation altitudes (below 30 m), this mean line is not quantitatively significant. However, it is most encouraging that it does lie in between the infinite height case and the strong ground effect case of the Crow-Bate theory. Since the actual magnitude of linking time differential for these two limit cases is not great, any fine-scale definition of the location of the mean line is not operationally significant.

Far greater operational significance should be placed on obtaining information relating to those (rare) cases in which the vortex persists beyond the time predicted by the Crow-Bate theory without either linking or spontaneous bursting. Such statistically rare events are the ones that are difficult to account for in a comprehensive analytical manner, and in the case of the vortex hazard, are the potentially most serious. None of these persistent vortices were observed in the present test program, however.

The Crow-Bate theory apparently sets an upper limit on the lifetimes of the vast majority of vortex wakes if the experimental agreement with the theory demonstrated here can be extrapolated to other aircraft scales. The previous experimental work by Tombach, et al (1974) did not demonstrate quite as close agreement with the theory as these data demonstrate, although a similar airplane and similar experimental techniques were used. One significant difference between the two experimental sets of results was in the measurement of turbu-

lence in the test region, however, which might account for the lesser scatter here. In the earlier experiments, turbulence was measured periodically near the test site by another aircraft and the results of these measurements were interpolated for turbulence at each specific test time. For the present series, the turbulence measuring equipment was contained aboard the generator aircraft which measured the turbulence directly in the test region and at the exact time of each of the experimental runs. Thus, it is felt that a far greater confidence can be placed on the values obtained for the turbulence here than from the previous tests.

Bursts. Two types of bursts were observed, those associated with linking and those which did not appear to be associated with any of the measured test parameters in an obvious way.

The link-associated bursts are identified separately in Figure 4-10. These bursts typically occurred several seconds before the linking process terminated and at a position on the vortex very near the link point. Investigations of this phenomenon were not carried beyond this, since core bursting was not of prime importance in this program, and core bursts after linking are not shown on the figure. Whether or not the basic mechanisms causing this link-associated bursting are different than those involved with other bursts is still a matter for conjecture.

Although the theory appears to set an upper limit on wake lifetime due to Crow instability, there are many instances when the initiation of wake destruction at earlier times was brought about due to spontaneous core bursting, as indicated by the open circles in Figure 4-10. This appears to be a truly random effect in the present tests, or if not random, at least the significant causal parameters are not known. Future investigations should clarify this.

The times associated with the bursts in Figure 4-10 are those times at which bursting at some point was first observed. It is not

the time at which the entire vortex experienced destruction. Significant segments of the vortex remain between burst points until they are consumed by the axially moving bursts. This is the case both for those vortices for which link-associated bursting occurs, as well as for those for which spontaneous, non-link-associated bursting is the destruction mechanism. Apparently, however, vortices are ultimately always destroyed by breakdown.

Such residual vortex segments, if positioned properly with respect to an encounter aircraft on final approach to a runway, could still constitute a significant hazard. An important parameter to obtain is the upper limit on wake lifetime after the vortices have been rendered completely harmless by breakdown, triggered either by the Crow instability, or earlier, by the regularly observed but as yet unexplained spontaneous bursting process. Such an analysis of all previous experimental data remains to be done.

5. CONCLUDING SUMMARY

The analyses in this report neatly fill out the spectrum of conditions to which the mutual induction instability of Crow and Bate can be applied, with formulations now existing for a wake in isotropic turbulence aloft ($h \gtrsim 4.3\ b_v$), for a wake in ground-influenced turbulence in the constant stress layer ($b_v \lesssim h \lesssim 4.3\ b_v$), and for a vortex interacting with its image in ground effect ($h = b_v/2$). These three theories are self-consistent and the limited experimental data available suggest the formulations are reasonable.

In general, the theories show that, in a given boundary layer, the net effect of ground proximity is to shorten wake lifetime, but by only 10% over the range $h/b_v = \infty$ to $h/b_v = 1/2$. The formulas which were developed apply to a constant height of the wake; since actual wakes change height as they develop, direct application of the formulas is not straightforward. The small change in lifetime over a large range of heights means, however, that use of the vortex generation height as the height for the calculations will always result in a slightly conservative estimate of wake lifetime.

There are some limitations inherent in the analyses which were performed here, which should be reviewed to put everything into perspective. The limitation due to an assumed constant height was discussed above and is minor. More important is the assumption that the region below $h \approx 4.3\ b_v$ is in the constant stress layer. As was emphasized in Chapter 2, under the calm and strongly stable conditions which are often of interest for operational applications, the stability suppresses the coupling through turbulence between the surface and levels aloft and thus the constant stress layer can easily be very thin -- say 10-20 m. Then the parameter η^* will not necessarily be constant throughout the region of interest, and in fact will be unknown from the top of the constant stress layer up to the level where isotropic turbulence can be assumed.

A specific limitation which applies to the interaction of the vortex and its image is the assumption that the wind is a crosswind. This limitation was applied because the magnitude of the horizontal turbulence varies with wind direction. As the discussion in Chapter 2 showed, however, there is no a priori reason for horizontal turbulence to follow any of the similarity laws and thus the experimental data shows wide scatter. The same data show the crosswind turbulence to be 10-20% less than the along-wind turbulence, but the difference is small compared to the error in estimating the turbulence in the first place. Thus for all practical purposes the analysis is valid for all wind directions.

One observation presented in this report is not new, but the perspective from which it is viewed is. Many previous investigations have shown vortex core bursting to be a decay mode which occurs frequently around the time of vortex linking due to the mutual induction instability, and often occurs at earlier times. After reviewing the current data, as well as previous experimental results, it has become clear that the core breakdown is the inevitable decay mode upon which the sinuous instability might be superimposed. The core breakdown can occur at any time, with its fundamental forcing mechanism still unknown. The frequently observed correlation with the linking (and hence with the turbulence) appears to be a consequence of vortex structure changes just prior to, and after, linking takes place. Thus bursting inevitably accompanies linking, while linking need not accompany bursting.

A decay in vortex strength as it travels in ground effect has been an item of conjecture for some time. In a prior experimental program one of the authors noted that the only time he ever saw the smoke-marked vortex dissipate, rather than decay through instabiltiy, was when they were traveling along the ground. Recent work by the U.S. Department of Transportation has also indicated a slow decay

of vortex strength in ground effect. Thus the measurements which were made here of the decay in the speed of vortex spreading in ground effect appear to corroborate these earlier observations. The rapidity of the decay in strength, which is proportional to the decay in separation speed, is suprising, as is its geometrical consistency.

In overall summary, the development of formulas for the prediction of the onset of wake decay by the sinuous mutual induction instability is probably complete. For operational purposes these formulas seem to be applicable within a factor of two or better for predicting wake lifetimes.* The uncertainty seems to be more related to the random nature of atmospheric structure than to any weaknesses in the theoretical formulation. Thus, further refinement of the theory, except possibly on the basis of some adjustment of constants based on a large volume of operational data, is probably unwarranted.

---

*See Tombach, Bate and MacCready (1974) for data aloft on this point.

REFERENCES

Bisgood, P. L., R. L. Maltby, and F. W. Dee (1971): Some Work on the Behavior of Vortex Wakes at the Royal Aircraft Establishment. In Aircraft Wake Turbulence and Its Detection, Ed. J. H. Olsen, et al, Plenum Press, New York.

Busch, N. E., and H. A. Panofsky (1968): Recent Spectra of Atmospheric Turbulence. Quart. J. Roy. Met. Soc., 94, 132-148.

_____, H. Tennekes, and H. A. Panofsky (1973): Turbulence Structure in the Planetary Boundary Layer. Boundary Layer Met., 4, 213-240.

Crow, S. C. (1970): Stability Theory for a Pair of Trailing Vortices. AIAA J., 8, 2172-2179.

_____, and E. R. Bate, Jr. (1975): Lifespan of Trailing Vortices in a Turbulent Atmosphere. J. Aircraft, to be published.

Fiedler, F., and H. A. Panofsky (1972): The Geostrophic Drag Coefficient and the Effective Roughness Length. Quart. J. Roy. Met. Soc., 98, 213-220.

Jones, J. J. P., and F. Pasquill (1959): An Experimental System for Directly Recording Statistics of the Intensity of Atmospheric Turbulence. Quart. J. Roy. Met. Soc., 85, 225-236.

Lamb, H. (1945): Hydrodynamics. Sixth Edition, Dover, New York

Lissaman, P. B. S., S. C. Crow, P. B. MacCready, Jr., I. H. Tombach, and E. R. Bate, Jr. (1973): Aircraft Vortex Wake Descent and Decay Under Real Atmospheric Effects. Final report to DOT, FAA, Systems R&D Service, Washington, D. C. Report No. FAA-RD-73-120. Available through NTIS.

Lumley, J. L., and H. A. Panofsky (1964): The Structure of Atmospheric Turbulence. Interscience Publishers, John Wiley and Sons, New York.

McBean, G. A. (1971): The Variations of the Statistics of Wind, Temperature and Humidity Fluctuations with Stability. Boundary Layer Met., 1, 438-457.

MacCready, P. B., Jr. (1962): The Inertial Subrange of Atmospheric Turbulence. J. Geophysical Research, 67, pp. 1051-1059.

REFERENCES (cont.)

Monin, A. S., and A. M. Obukhov (1954): Basic Regularity in Turbulent Mixing in the Surface Layer of the Atmosphere. Trudy Geofiz. Inst. Akad. Nauk. SSSR, 24, 163-187.

Panofsky, H. A., and F. Pasquill (1963): The Constant of the Kolmogorov Law. Correspondence from Quart. J. Roy. Met. Soc., 89, 382, 550-551.

Pasquill, F. (1972): Some Aspects of Boundary Layer Description. Quart. J. Roy. Met. Soc., 98, 469-494.

Tennekes, H., and J. L. Lumley (1972): A First Course in Turbulence. The MIT Press, Cambridge, Mass.

Tombach, I. T. (1974): Influence of Meteorological Factors on the Vortex Wake of a Light Twin-Engine Aircraft. AFOSR Technical Report AFOSR-TR-74-1507.

_____, E. R. Bate, Jr., and P. B. MacCready, Jr. (1974): Investigation of the Motion and Decay of the Vortex Wake of a Light Twin-Engine Aircraft. AeroVironment Inc. Final Report FR 439 to Dept. of Transportation, Transportation Systems Center under Contract DOT-TSC-523.

Tritton, D. J. (1967): Some New Correlation Measurements in a Turbulent Boundary Layer. J. Fluid Mech., 28, 446.

Widnall, S. E. (1974): The Structure and Dynamics of Vortex Filaments. Annual Review of Fluid Mechanics, Annual Reviews Inc., Palo Alto, 141-166.